Fusion Approaches to Individual Tree Species Classification Using Multi-Source Remotely Sensed Data

Qian Li

A Thesis Submitted to
The Faculty of Graduate Studies
In Partial Fulfillment of the Requirements
for the Degree of
Master of Science

Graduate Program in
Earth and Space Science and Engineering
York University
Toronto, Ontario

May 2022

Abstract

Tree species information plays essential roles in urban ecological management and sustainable development, and thus tree species classification has been an active research topic over the years. This study investigated fusion approaches deployed with Support Vector Machine (SVM) and Random Forest (RF) algorithms to incorporating multispectral imagery (MSI), a very high spatial resolution panchromatic image (PAN), and Light Detection and Ranging (LiDAR) data for five object-based tree species classification in an urban environment. The results demonstrated that 3D structural features contributed more to tree species with broad crowns, such as honey locust and Austrian pine, whereas textural features were more effective in differentiating trees in narrow crowns, such as spruce. Among all the possible classification schemes based on multi-source features in combinations, decision fusion achieved the best overall accuracies (0.86 for SVM and 0.84 for RF), slightly outperforming the feature fusion approach (0.85 for SVM and 0.83 for RF). Both fusion approaches significantly improved tree species classifications produced by MSI (0.7), PAN (0.74), and LiDAR (0.8) individually.

Acknowledgments

I would like to extend my sincere appreciation to many people for their encouragement and help throughout my academic journey in the Master's program. It will be a precious experience of growing and exploring in my life.

I want to first express my deep gratitude to my supervisor, Dr. Baoxin Hu. Her constructive suggestions and patience were greatly appreciated while working on this thesis. To be honest, I have learned a lot from her on academic writing. Her rigorous academic attitude and positive life experience inspired me to explore my potential in research.

I am deeply thankful to Dr. Jiali Shang for providing helpful advice and generous support. Her positive attitude and her laugh are infectious. I would also like to thank my graduate committee members, Dr. Mark Gordon and Dr. Tarmo Remmel, for the valuable comments and research evaluation. And I especially thank Dr. Yongsheng Chen for enlightening me on the research and life practice.

I appreciate having many excellent friends and colleagues, Wen Zhang, Ima-Obong Ituen, Rory Pittman, Chen Xing, Andy, and Farah, around for help and support. In particular, I would like to express my great thanks to Dr. Hui Li for her help in the image registration and Dr. Zhouxin Xi for teaching me a lot. Attending the 40th CSRS conference was a great unforgettable experience.

Last, the most profound gratitude goes to my family. Their unconditional love and understanding encourage me to pursue my dreams. A huge thanks to my husband, Junjie Kang, for supporting and accompanying me over the years.

I also should thank the York University library and for LiDAR data and Campus Services and Business Operations (CSBO) for tree inventory. I want to acknowledge the funding support of this thesis research from the Natural Sciences and Engineering Research Council (NSERC) of Canada, Esri Canada, and the Ontario Ministry of Agriculture, Food and Rural Affairs (OMAFRA).

Table of Contents

List of Tables

List of Figures

Chapter 1 Introduction

Trees are vital components of the urban ecosystem. They deliver a multitude of environmental, ecological, and social services, including reducing noise and air pollution, preventing soil erosion and flooding, mitigating the effects of urban heat islands, and improving human well-being (Huang, 2019). However, the provision and optimization of ecosystem services are significantly reliant upon the richness of tree species in urban ecosystems (Morgenroth et al., 2016). Tree diversity also improves the resistance and resilience to disturbances such as climate change, pests, and disease in urban forests in the long term. To promote tree diversity and further optimize ecosystem services for the residents, knowledge of the current state of tree species in urban areas is needed to make informed decisions. It has been demonstrated that accurate tree species classification can provide needed information for sustainable city planning, ecological management, and a variety of studies, such as air pollution studies focusing on specific tree species largely influencing the air quality (Fitzky et al., 2019), development of resource inventory (Denisova et al., 2019), biodiversity assessment and conservation (Felton et al., 2020), invasive species detection and monitoring (Piiroinen et al., 2018), pest and disease monitoring (Paap et al., 2017), as well as the overarching goal of sustainable urban forest management (Larrubia et al., 2017).

Tree species composition has been conventionally collected through field surveys and visual interpretations of aerial photographs, often restricted to small areas. These methods are labor-intensive, time-consuming, and inefficient in practice (Shojanoori & Shafri, 2016). Remote sensing has been applied as a cost-efficient alternative to classifying

urban tree species with varying degrees of success over multiple scales for several decades (Fassnacht et al., 2016). The challenge in tree species classification using remotely sensed data is mainly due to the complexity of forest canopies in terms of their physical and biophysical properties (Hu et al., 2021). In remotely sensed data, trees of the same species may exhibit different properties, but trees of different species may show similar properties. This is likely true with specific features derived from a single data source, such as spectral signatures commonly used in remote sensing classification. This problem may be minimized when several types of data (or features) are utilized. However, the utilization of multi-source remotely sensed data is challenging researchers in terms of fully exploiting individual datasets and integrating multi-source information. The goal of this thesis was to exploit the discriminant power of individual datasets and seek an effective way to combine information from different sources.

Generally, tree species identification using remotely sensed data includes two major aspects: feature extraction and classification. In feature extraction, features reflecting attributes of tree canopies, such as color, texture, and shape, are derived from remotely sensed data, also known as remote sensing features. Classification is typically conducted on the extracted features to categorize image pixels into tree species classes.

In terms of feature extraction, four types of features, including spectral, textural, structural, and temporal, are mostly considered in species classification using remotely sensed data. Spectral and textural features are mainly extracted from multi-spectral/hyperspectral imagery based on the reflectance in specific wavelength bands (Mojaddadi Rizeei et al., 2019). The commonly used spectral features include reflectance

of individual pixels for pixel-based classification and mean reflectance and its standard deviation for the classification based on individual tree crowns. (Hartling et al., 2019; D. Li et al., 2015; Liu et al., 2017; Shi, Skidmore, et al., 2018). In addition, vegetation indices (e.g., Normalized Difference Vegetation Index (NDVI) and Enhanced Vegetation Index (EVI)) are also widely utilized for tree species classification (Kukunda et al., 2018; Liu et al., 2017; Marrs & Ni-Meister, 2019).

Textural features usually reflect the spatial variations in the reflectance within individual tree crowns or a given region of interest by quantifying the frequency and distribution of the reflectance values (Franklin et al., 2001). Statistical grey level co-occurrence matrix (GLCM) is the most popular texture analysis method (Ferreira et al., 2019; Haralick et al., 1973). Metrics calculated from GLCM such as homogeneity, contrast, correlation, and energy are commonly used (Aval et al., 2019; Ferreira et al., 2019; Stavrakoudis et al., 2014). However, a comprehensive investigation of GLCM-based textural measures including broad feature types is needed. In addition, features based on other texture analysis techniques, such as those derived using Gabor filters, are rarely used in tree species classification, although they have been widely utilized for texture segmentation and classification (Yang et al., 2019).

Structural features are mainly derived from LiDAR (Light Detection and Ranging) data (Li et al., 2013, 2015). 3-dimensional (3D) data acquired by a LiDAR instrument with its capability of penetrating tree canopies can be used to describe their crown shape and the vertical distribution of branches and foliage. LiDAR-derived features can be broadly grouped into two dominant categories: 1) describing general tree crowns, such as maximum

tree height, the shape and size of tree crown etc. (Aval et al., 2019; Dalponte et al., 2012), 2) reflecting detailed foliage distributions within crowns, such as the proportions of individual returns, 2D and 3D statistics of LiDAR 3D points distribution (Li et al., 2013, 2015; Lin & Martin, 2016). Various successes have been reported in the literature in individual tree species classification using a number of these LiDAR-derived features (Li et al., 2013, 2015; Lin & Hyyppä, 2016; Shi et al., 2018). However, Aval et al. (2019) reported a marginal contribution of height-related structural features derived from LiDAR data in individual tree species classification; LiDAR-derived features exhibited an overall accuracy of 31% and hampered the classification performance when integrated with spectral and textural features. It must be noted that Aval et al. (2019) highlighted the importance of extracting the most relevant features prior to merging the complementary multi-source remote sensing data. Therefore, more attention is needed to investigate the advanced 3D structural features such as point distribution-related features for multi-source remote sensing-assisted classification in urban forests.

Temporal features are captured from multi-temporal remote sensing data according to seasonal variation associated with tree species characteristics, such as leaf shedding and color changes of broadleaved trees in autumn (Fang et al., 2018). Temporal features depend primarily on the revisit time of sensor systems, and they are not included in the current study. It is worth mentioning that with the improvements in spatial resolution of remote sensors, features are often extracted from individual tree crowns rather than pixels for tree species classification (Wang et al., 2018). These features mentioned above are used for classification either individually or in combination, which will be described in detail after

reviewing classification methods.

In terms of classification techniques, they have evolved with the technological advancements in the computational capacity and easy accessibility of statistical learning tools such as R, MATLAB, and scikit-learn for Python (Fassnacht et al., 2016). Commonly used classification algorithms in remote sensing include Maximum Likelihood, k-nearest neighbors (KNN), Decision Trees Classifier, Support Vector Machine (SVM), Random Forests (RF), Boosted Trees Classifier, and Artificial Neural Networks (Deep Learning). Over the last two decades, there has been an increasing trend of using nonparametric machine learning algorithms such as SVM and RF to separate tree species considering their significant computing capacities and freedom from the normal distribution requirement of the input dataset (Raczko & Zagajewski, 2017). As mentioned earlier, spectral, textual, and structural features derived from multi-source remotely sensed data are used in tree species classification individually or in combination in the literature. With a massive number of data readily available from various sensors, fusion-based classification approaches have been an important ongoing research topic (Aval et al., 2019; Fassnacht et al., 2016; Hartling et al., 2019, 2021; Liu et al., 2017; Stavrakoudis et al., 2014). Fusion typically occurs at either feature or decision level. Feature fusion aggregates features from individual data sources to create a combined feature vector for subsequent classification. For fusion at the decision level, features extracted from the respective data source are used for classification first, and the classification results are then merged at the decision level to obtain a final classification result.

Most existing studies employing fusion approaches incorporate multi-source data

at the feature level (Alonzo et al., 2014; Dalponte et al., 2012, 2019; Hartling et al., 2019, 2021; H. Li et al., 2020; Liu et al., 2017; Pu & Landry, 2012). For example, Pu & Landry (2012) combined spectral and GLCM-based textural features from IKONOS and WorldView-2 multispectral imagery to separate seven urban tree species/groups. Pu & Landry (2012) indicated the insufficiency of the used spectral and textural features considering the relatively low classification accuracy that could not satisfy the general requirement in most applications. Liu et al. (2017) employed LiDAR-derived structural features (crown shape, the distribution of LiDAR points within individual tree crowns, and laser return intensity-related features) in a combination of hyperspectral-extracted spectral features (reflectance and vegetation indices) to classify 15 common urban tree species using a RF classifier. Their results showed that classification using spectral and structural features individually yielded an overall accuracy of 51% and 61%, respectively, but the accuracy was increased to 70% with the combined features. Hartling et al. (2021) also demonstrated that additional structural information from LiDAR (height statistics and intensity) filled the information gap needed to distinguish tree species. Nevertheless, the high dimensionality in the feature space that results from feature-level fusion is likely to be a concern for applications where the size of training samples is small (Maxwell et al., 2018). In addition, features derived from different data sources are treated equally by the SVM and random forest methods, even though some of the data sources may be more reliable than others (Hu et al., 2021).

Several studies have recently investigated fusion at the decision level for species classification, and the advantages of decision-fusion over feature-fusion were

demonstrated. (Aval et al., 2019; Hu et al., 2021; Stavrakoudis et al., 2014). Stavrakoudis et al. (2014) mapped five forest species using the combined hyperspectral and multispectral imagery, and it showed that the decision level fusion exhibited a higher degree of flexibility and accuracy than the fusion at the feature level. Aval et al. (2019) carried out a decision fusion based on the posterior probabilities of trees belonging to a specific species from individual data sources. Although the decision fusion approach slightly outperformed the feature fusion in their study, Aval et al. (2019) recommended the use of decision fusion. Most recently, Hu et al. (2021) developed a decision fusion approach based on the Dempster Shafer theory (DST) to classify five urban tree species, which took into account all available pieces of evidence and associated uncertainties from multi-source remotely sensed data. Aval et al. (2019) and Hu et al. (2021) highlighted that it was important but difficult to define an appropriate decision rule to merge different data sources. An in-depth analysis of decision fusion approaches is needed to realize its potential in species classification.

In this thesis research, a systematic and in-depth investigation was carried out to thoroughly exploit the discriminatory powers of derived features and corresponding individual datasets, and effectively improve individual tree species classification of five dominant tree species using multi-source remotely sensed data. The followings are the specific objectives for this investigation.

(1) Exploit advanced textural and structural features for individual tree species classification.

Literature review shows that advanced textural and structural features derived from

high spatial resolution PAN and LiDAR data respectively warrant further investigation. In addition to spectral features and commonly used GLCM metrics, textural features calculated using Gabor filter techniques were extracted and tested for classification. Moreover, less commonly-used GLCM metrics were also assessed. Advanced 3D structural features were derived from LiDAR point cloud data to characterize the vertical and horizontal structure of individual tree crowns, including percentiles of point distribution along the vertical height profile, gap distribution represented by proportions of different return numbers, and 3D texture analysis based on the 3D distribution of LiDAR points inside the tree crown volumes. Feature selection was also carried out to determine the feature importance ranking of individual features and select crucial features for the feature-level fusion.

(2) Assess various classification schemes at feature-level fusion using spectral, textural, and structural features derived from MSI, high spatial resolution PAN, and LiDAR data.

A series of classification schemes were conducted using individual feature groups and various combinations to evaluate the classification performance of the feature-level fusion approach. The discriminatory power of each feature group was also identified to have a deep understanding of features' contribution to the accurate classification.

(3) Develop a DST-based decision fusion framework using probabilistic SVMs and RFs

The DST-based decision fusion process (Dempster, 1967; Shafer, 1976) can measure and consider the uncertainty and imprecision of each dataset in the multi-source classification decision-making stage (Hu et al., 2021). Most importantly, the DST-based

decision fusion approach has the potential for continual improvement of the classification performance when additional features become available, which provides a novel and open framework for individual tree species classification. A misclassification analysis of the results from the decision fusion and feature fusion was also conducted to provide insights on further improvement. In addition, the feature fusion and decision fusion approaches were also compared.

This thesis is structured into the following six chapters. In Chapter 1, the goal and objectives of the thesis research are introduced. Presented in Chapter 2 are the current relevant research and background information, specifically on feature extraction, feature selection, classification methods, and fusion strategy of multi-source remotely sensed data in the context of classification. The study area and data used in this research are described in Chapter 3. The data processing and co-registration between optical imagery and LiDAR data are included in this chapter. The methodology, including the derivation of spectral, textural, and structural features of individual tree crowns, feature selection, and classification, is described in Chapter 4. Chapter 5 presents the classification results and discussions. Lastly, in Chapter 6, the outcomes of the thesis research are summarized under the proposed objectives. The recommendations for future study are also provided in Chapter 6.

Chapter 2

Background

2.1 Tree Species Classification from Multi-Source Remotely Sensed Data

The rapid advancements in remote sensing technologies have made an increasing amount of data readily available from a wealth of sensors (e.g., high-resolution multispectral, hyperspectral, and LiDAR systems). Multi-source remotely sensed data have been extensively adopted in tree species classification over the last decade, commonly conducted between optical imagery and LiDAR data (Fassnacht et al., 2016; Shojanoori & Shafri, 2016; Wang et al., 2018). Multiple types of features, usually including spectral, textural, and structural signatures collected by optical imagery and LiDAR data, are capable of revealing tree species-related traits of individual trees from different perspectives. Complementary information from multi-source remotely sensed data has been the main driver in separating tree species.

Due to the need for the separation of individual tree crowns, high-spatial resolution multispectral imagery (hereafter referred to as MSI) is commonly used for individual tree species classification, such as that obtained by IKONOS (Pu et al., 2012), QuickBird (Gillespie et al., 2017), GeoEye (Aguilar et al., 2014), RapidEye (Tigges et al., 2013) and WorldView-2 (WV-2) (Hartling et al., 2019; Kukunda et al., 2018; Waser et al., 2014). In particular, high-resolution MSI from WV-2 has shown the most significant potential and suitability for the identification of individual tree species in urban environments

(Shojanoori & Shafri, 2016). The eight multispectral bands could offer plentiful spectral information, and the very high spatial resolution panchromatic band (hereafter referred to as PAN) could reveal the detailed spatial arrangement of elements within individual tree crowns. For instance, two datasets of satellite MSI from IKONOS and WV-2 were utilized to derive spectral and textural features for the classification of six urban tree species/groups in Florida, USA (Pu & Landry, 2012). The high spatial resolution and additional bands of WV-2 imagery resulted in a better classification accuracy of 63% (Kappa 0.45) in comparison with IKONOS imagery. Pu and Landry (2012) also indicated that background and shadow resulting from the complexity and heterogeneity of urban environments might reduce the spectral variations between tree species. Therefore, additional efforts should be made to improve the relatively low classification accuracy obtained from the classification using MSI. Although hyperspectral imagery may detect subtle differences in spectral signatures among species, its high cost and data volume, the complexity of data acquisition and processing, and the limited availability impede its widespread application in the context of tree species classification.

Shojanoori and Shafri (2016) indicated that LiDAR data is the most promising source to enhance tree species recognition in urban environments when combined with MSI. LiDAR systems are capable of generating 3D coordinates of targeted objects and can capture structural details of tree crowns that optical imagery fails to identify. The point cloud data provided by LiDAR systems usually includes 3D coordinates, intensity, and return numbers. 3D structural features can be derived from point cloud data to reflect the internal foliage and branch patterns of individual tree crowns, complementing spectral and

textural features in 2D obtained from MSI (Shojanoori & Shafri, 2016; Wang et al., 2018). Many existing studies have demonstrated the positive contribution of LiDAR data in conjunction with MSI for the purpose of improving tree species discrimination (Dalponte et al., 2012; Hartling et al., 2019; Kukunda et al., 2018; Saeidi et al., 2014). For example, Dalponte et al. (2012) illustrated the importance of using high-density LiDAR data (8.6 points per m^2) together with MSI. In their study, statistical parameters such as maximum, mean, standard deviation, and percentiles of height information of LiDAR points were derived to describe the structural characteristics of trees in a forest. Liu et al. (2017) observed a significant improvement in classification accuracy from 51.1% to 70.0% when incorporating LiDAR data into hyperspectral imagery to classify 15 common tree species in the city of Surrey. Most recently, Hartling et al. (2021) demonstrated that given limited spectral information, additional structural information from LiDAR (height statistics and intensity) filled the information gap needed to distinguish tree species.

2.2 Feature Extraction from MSI, PAN, and LiDAR Data

In tree species classification using remotely sensed data, spectral, textural, and structural features derived from MSI, PAN, and LiDAR data, respectively, are commonly used. The variability of spectral reflectance determined by specific biochemical and biophysical properties of different tree species is the primary driver behind tree species classification using MSI (Fassnacht et al., 2016). Textural features from very high spatial resolution PAN describe the variations in the reflectance within individual tree crowns, reflecting information on spatial and physical arrangements of tree elements, such as branches and foliage (Yang et al., 2019). Structural features extracted from LiDAR data

have the capacity to represent the internal structure properties along the vertical profile of a single tree on the basis of the point distribution information in 3D (Aval et al., 2019; Dalponte et al., 2012; Li et al., 2013). These three feature groups are discussed in further detail below.

2.2.1 Spectral Features

Spectral features represent the characteristic of spectral reflectance in the optical region of individual tree crowns in the context of individual tree species classification. In the visible region of the spectrum (400–700 nm), the dominant factors controlling leaf reflectance include various leaf pigments in the palisade mesophyll (e.g., chlorophyll *a* and *b*, and β-carotene), which presents the primary chlorophyll absorption features at the blue (430-450 nm) and red (650-660 nm) bands (Asner, 1998; Clark & Roberts, 2012). In the near-infrared region of the spectrum (700–1300 nm), the scattering of the near-infrared radiation in the spongy mesophyll of leaves typically causes the strong reflectance at this wavelength interval (Asner, 1998). In the mid-infrared region of the spectrum (1300–2500 nm), leaf water content dominates three primary water absorption features at 1450 nm, 1940 nm, and 2700 nm (Waser et al., 2014). Tree structures (e.g., leaf and branch density, angular distribution, and clumping) also affect the reflectance at the canopy level and the background, such as the bare soil and understory vegetation (Spanner et al., 1990). Spectral features used in species classification include the reflectance at individual spectral bands and a variety of vegetation indices. These spectral features are described in detail in section 4.1.1. Vegetation indices are developed to maximize the sensitivity to biophysical and biochemical parameters of vegetation and minimize confounding factors such as soil

background reflectance or atmospheric effects (Kukunda et al., 2018; Liu et al., 2017; Marrs & Ni-Meister, 2019). The commonly used vegetation indices include NDVI, green NDVI, red edge NDVI (Gitelson & Merzlyak, 1994), the optimized soil-adjusted vegetation index (OSAVI) (Rondeaux et al., 1996; C. Wu et al., 2014), and the enhanced vegetation index (EVI) (Huete et al., 2002; Madonsela et al., 2017). Many studies, however, have illustrated that spectral information alone is insufficient to separate tree species (Aguilar et al., 2014; Gillespie et al., 2017; Hartling et al., 2019; Pu & Landry, 2012). This is mainly due to the fact that spectral reflectance of individual tree crowns varies with many factors such as foliage age and its health status, leaf area density, canopy structures, and background (Clark et al., 2005; Clark & Roberts, 2012). Trees of the same species may exhibit different spectral features, while different tree species may have similar spectral signatures.

2.2.2 Textural Features

Textural features has been successfully derived from panchromatic image to represent important textural information for tree species classification in the literature considering its very high spatial resolution (Aval et al., 2019; Fang et al., 2018; Ferreira et al., 2019; Hartling et al., 2019). Existing methods for the extraction of textural features are broadly classified into four categories: statistical, structural, model-based, and transform-based methods (Bharati et al., 2004). Among them, statistical approaches such as GLCM (Haralick et al., 1973) are the most popular and conventional (Aval et al., 2019; Ferreira et al., 2019; Haralick et al., 1973; Stavrakoudis et al., 2014). A detailed description of these measures is provided in Table 4-4.

GLCM characterizes the relationship in the reflectance among neighboring pixels (Haralick et al., 1973), which considers the co-occurrence of pairs of reflectance between two pixels separated by a given distance and at a given direction to obtain the second-order textural statistics, such as contrast, correlation, energy and homogeneity. A number of metrics based on GLCM have been proposed to describe the textures of various objects. Initially, 14 textural measures were computed from GLCM to classify sandstones and many types of land-use categories (e.g., forest, woodlands, grasslands, urban areas, and water bodies) Haralick et al. (1973). Soh and Tsatsoulis (1999) proposed five additional GLCM-based features for textural measures and classification: cluster prominence, cluster shade, dissimilarity, autocorrelation, and maximum probability. Clausi (2002) contributed two more features based on GLCM: inverse difference normalized and inverse difference moment normalized (Clausi, 2002). The original measures proposed by Haralick et al. (1973) are commonly used in tree species classification. Ferreira et al. (2019) reported the improvement of tree species classification in tropical forests when combining eight of Haralick's GLCM-based textural features, including mean, variance, homogeneity, contrast, dissimilarity, entropy, second moment, and correlation, using a pan-sharpened VNIR band of WorldView-3 satellite imagery. Aval et al. (2019) employed similar Haralick's textural statistics from PAN to differentiate 15 tree species at the crown level in conjunction with spectral information from MSI and structural features from LiDAR data, and it was observed that textural features significantly contributed to the identification of two tree species (*Tilia tomentosa* and *Platanusxhispanica*) with high accuracy. However, other GLCM features, such as cluster shade, cluster prominence, and inverse difference

normalized, were rarely used in tree species classification.

In comparison with the GLCM method, the transform-based Gabor filters are less common in remote sensing-assisted classification. Gabor filters are designed to emulate the characteristics of the human visual system in which an image formed in the retina is decomposed into several filtered images with a specific range of spatial frequencies and orientations (Daugman, 1985). Gabor filters are robust against varying brightness and contrast of images. 2D Gabor filters have been used for textural representation and discrimination in pattern recognition (Haghighat et al., 2013; Ramakrishnan et al., 2002; Yang et al., 2019). This study used Gabor filters to describe the texture of individual tree crown regions in PAN. The calculation process presented in Zheng et al. (2004) was employed (Zheng et al., 2004). A 2D Gabor filter in the spatial domain is defined in Eq. (2-1).

$$h(x,y;f,\theta)=\frac{1}{\sigma\sqrt{2\pi}}\exp(-\frac{x^2+y^2}{2\sigma^2})\cdot\exp(if(x\cos\theta+y\sin\theta)), \quad (2\text{-}1)$$

where x and y are the coordinates of a given pixel in the image; the parameter σ is the standard deviation of the 2D-Gaussian function in the x and y directions; f is the central frequency of a sinusoidal wave; θ is the spatial orientation of the filter.

For Gabor textural feature extraction, the image *I* is convolved with each Gabor filter created with specific orientations and frequencies at every pixel (*x, y*) based on Eq. (2-2).

$$G(x,y;f_k,\theta_m)=\sum_{x'}\sum_{y'}I(x-x',y-y')h(x',y';f_k,\theta_m), \quad (2\text{-}2)$$

where *I (x, y)* is the grey value distribution of the image *I*; and $G(x,y;f_k,\theta_m)$ is the

convolution result corresponding to the Gabor function at the orientation denoted by *m* and the frequency denoted by *k*. In the current study, the square energy and mean amplitude were calculated as textural features from the output image $G(x, y; f_x, \theta_m)$ to measure the textural variation based on the specific frequency content in specific directions in a tree crown region of analysis. The mean amplitude of $G(x, y; f_x, \theta_m)$ provides the oriented frequency spectrum in each local of a tree crown region in PAN, as defined in Eq. (2-3).

$$\text{GaborFilter}_{\text{A}}(x, y; f_x, \theta_m) = \overline{|G(x, y; f_x, \theta_m)|} \quad (2\text{-}3)$$

Another textural feature, square energy, denotes the local energy of the frequency response in a specific orientation of a tree crown region in PAN. Square energy was computed as:

$$\text{GaborFilter}_{\text{E}}(x, y; f_x, \theta_m) = \sum \text{GaborFilter}_{\text{A}}(x, y; f_x, \theta_m)^2 \quad (2\text{-}4)$$

2.2.3 Structural Features

Trees of different species may have different arrangements of foliage and branching structures (Fassnacht et al., 2016; Li et al., 2013; Wang et al., 2018). For instance, an Austrian Pine (*Pinus nigra*) tree typically forms a semi-round shape with broadly spreading branches and clusters of leaves along the trunk, and the branches and foliage of blue spruce (*Picea pungens*) or white spruce (*Picea glauca*) are often uniformly distributed around the trunk with dense layers from the side view, and they have the distinctive pyramidal shapes. Therefore, various structural features have been derived from LiDAR data to improve the classification accuracy of individual tree species (Li et al., 2013, 2015; Lin & Hyyppä, 2016; Shi et al., 2018). Existing LiDAR-derived features for tree species classification are derived to describe both general geometric shapes of individual tree crowns and the detailed distribution of tree elements of each tree crown (Aval et al., 2019; Dalponte et al.,

2012; Liu et al., 2017; Reitberger et al., 2008; Yao et al., 2012). For the former, features include statistical parameters such as maximum, mean, standard deviation of the normalized height, crown area based on the 2D convex hull, and ratios of the projected crown area to the tree height of laser points within a tree crown. (Shi et al., 2018). Yao et al. (2012) indicated that three geometric LiDAR features, including crown base height, crown volume, and crown area, were promising structural features for better tree species classification performances, especially for deciduous trees. Features describing the internal structures of individual tree crowns are designed to quantify the distributions of LiDAR 3D points within crowns in both horizontal and vertical directions. These features include percentiles of point distribution along with the vertical height profile (Lin & Hyyppä, 2016; Puttonen et al., 2010), proportions of different return numbers (Shi et al., 2018), and 3D texture analysis (Li et al., 2013). The use of LiDAR-derived features has been beneficial to individual tree species classification. For example, Li et al. (2013) employed such features as 3D texture, gap distribution, the degree and scale of foliage clumping along with tree height horizontally and vertically to classify four tree species in a forest region; an overall classification accuracy of 77.5% (Kappa 0.7) was achieved and it demonstrated the significant contribution of structural features to tree species classification. Most recently, Liu et al. (2017) demonstrated a positive contribution of LiDAR point distribution-related features when classifying 15 common urban tree species based on hyperspectral imagery and LiDAR point cloud data. In combination with LiDAR-derived structural features, including crown shape, laser point distribution, and intensity-related features, they attained an improvement of nearly 20% in the overall accuracy.

In addition, LiDAR intensity has been employed in tree species classification as well (Korpela et al., 2010; Lin & Hyyppä, 2016; Liu et al., 2017; Shi et al., 2018). Lin and Hyyppä (2016) derived the average intensity value of LiDAR laser points at different height quantiles and the statistics of the intensity values regarding laser points belonging to a tree crown for tree species classification. Similarly, Shi et al. (2018) computed radiometric features associated with intensity and echo width under leaf-on and leaf-off conditions. Compared with spectral features derived from the multispectral or hyperspectral imagery, spectral information captured by LiDAR systems is based on a narrow wavelength mainly located in the near-infrared spectrum (Wang et al., 2018). Moreover, the complexity of radiometric calibration establishing the relationship between actual physicochemical properties of tree canopies and raw intensity values from LiDAR sensors prevents the practical applications for the identification of tree species, although some studies have shown promising classification results with radiometric features when only LiDAR data was available (Kashani et al., 2015).

2.3 Feature Selection

Feature selection is commonly implemented prior to the classification to select a subset of essential features by removing redundant or irrelevant ones (Georganos et al., 2018). Feature selection is essential for classification especially when multi-source remotely sensed data is used where the number of features tends to be very large. Due to noise and uncertainty in data, a larger number of features might not produce higher classification accuracy, and the important features might be masked out by “unnecessary” ones, leading to reduced accuracy (Gregorutti et al., 2017). In addition, with the increase

of the number of features, the number of training samples needs to be increased, but training samples are difficult to obtain in practice. Among the existing feature selection methods, recursive feature elimination (RFE) combined with a RF classifier was highlighted by a number of studies in the literature as it can provide an unbiased feature selection and effectively increase classification accuracy (Demarchi et al., 2020; Georganos et al., 2018; Gregorutti et al., 2017). Specifically, Gregorutti et al. (2017) recommended the use of the RFE algorithm, considering its good performance, even in the presence of correlated features. Demarchi et al. (2020) reported that RFE effectively handled the fusion of complementary and diverse data sources, such as hyperspectral imagery and LiDAR data. In this thesis research, the RFE wrapped with RF was implemented to select relevant features and assist the interpretation of feature contribution to classification accuracy.

A critical aspect of any feature selection method is the measure of the importance of given features. In the RFE wrapped with RF, mean decrease in accuracy (MDA) is commonly used to evaluate the importance of features using training samples (Breiman, 2001). MDA is produced using the following steps: 1) each tree (in the RF) is trained with a random subset of the input features and one-third of the training data, namely the out-of-bag (OOB) samples that are used to estimate the classification error; 2) the classification error on the OOB samples is calculated for each tree in RF, and the same is done after randomly permuting each features value; and 3) MDA of a feature is computed by averaging the differences between the two classification errors over all trees in RF using Eq. (2-5) (Han et al., 2016). The more significant value of the decrease in accuracy

indicates the more important the feature is in the classification model, and vice versa.

$$MDA_i = \frac{1}{n_{tree}} \sum_{n=1}^{n_{tree}} (E_i - E_{i'}) \quad (2\text{-}5)$$

where n_{tree} is the number of trees in RF, E_i refers to OOB error in tree n before permuting the value of feature i, and $E_{i'}$ denotes the OOB error in tree n after permuting the value of feature *i.*

2.4 Classification Methods

2.4.1 Support Vector Machine and Random Forest

The utility of machine learning algorithms has significantly facilitated tree species classification from remotely sensed data due to its advances in computational efficiency, statistical learning capability, and easy access to hardware and software such as R and scikit-learn for Python (Chang & Bai, 2018; Fassnacht et al., 2016). Machine learning algorithms have the capacity to model a high-dimensional feature space and classify tree species with very complex characteristics represented by multi-source remotely sensed data. These distribution-free or nonparametric algorithms are usually more adequate for multi-source classifications. Among the various machine learning algorithms, SVM and RF have been demonstrated to be more robust for classification with a large number of features in comparison with other traditional methods, such as maximum likelihood and KNN classifiers. (Fassnacht et al., 2016; Maxwell et al., 2018). According to the statistics in the related literature review, Fassnacht et al. (2016) indicated that SVM and RF are at the top of the most frequently used classification algorithms in remote sensing. Most importantly, Maxwell et al. (2018) summarised that RF and SVM offered good

performance with low computational cost after experimenting with multiple commonly used classifiers. Moreover, probabilistic outputs computed by SVM and RF can facilitate the DST-based decision fusion approach for tree species classification.

In order to identify suitable classifiers for the tree species dataset in this study, logistic regression, KNN, single decision tree, RF, SVM, and Naive Bayes algorithms available in R software were implemented on the training dataset to test their classification performances. The results showed that SVM and RF outperformed the other classification algorithms in terms of overall classification accuracies. In this thesis study, SVM and RF were adopted to implement the supervised classification and deployed with fusion approaches to individual tree species identification, which combines MSI, high-resolution PAN, and LiDAR point cloud data.

SVM has been highlighted in the applications of complex classification problems such as tree species differentiation (Aval et al., 2019; Hartling et al., 2019, 2021; Stavrakoudis et al., 2014; Wu & Zhang, 2020). SVM was initially introduced as a binary classifier and extended to multi-class classification (Mountrakis et al., 2011). The multi-class classification problem is breakdown into multiple binary classification cases using a strategy of either “one against all” or “one against one” (Karatzoglou et al., 2006; Meyer & Wien, 2021). The “one against all” classification builds a binary classifier model (N models if N is the number of tree species classes) for each class and trains them to separate samples in a class from samples in all remaining classes. The “one against one” approach builds and trains a binary classifier model for each pair of classes (N(N-1)/2), which was used in the current study. The class with the most frequent wins over all possible binary

classifiers is assigned to a given sample. SVM is initially designed for linear problems. Kernel methods, also known as “kernel tricks”, including the linear kernel, polynomial kernel, sigmoid kernel, and radial basis function (RBF), enable the inherent linear SVM to perform non-linear classification by implicitly transferring the original feature space to a higher dimensional space that is linearly separable by the algorithm. With non-linear kernels, SVM is widely accepted in patterns of remote sensing data-based classifications. Two commonly used optimum parameters need to be considered to build robust and accurate classification models using kernelized SVM since they are essential in preventing the classifier from overfitting or underfitting. One is the cost parameter (c), which is applied to fix the misclassification caused by a hard decision boundary by creating a complex classification function with the least misclassification (Karatzoglou et al., 2006). Another parameter (gamma) is considered as the width parameter of the kernel that reshapes the decision boundary and decision region by controlling the complexity of the classification function (Karatzoglou et al., 2006). On the other hand, Maxwell et al. (2018) reported an adequate classification performance using the default parameters (c and gamma) instead of optimizing parameters using machine learning algorithms such as SVM and RF which are robust to parameters settings.

Furthermore, SVM classifiers can produce posterior probability values quantifying the confidence that a sample belongs to each class instead of predicted class labels (Lin et al., 2007). For binary SVM, the probability is calculated using the Platt scaling method (Platt, 1999), which approximates the posterior probability by fitting a logistic distribution to decision values using maximum likelihood on the training dataset. The current study

employed the posterior class probabilities for multi-class classification computed using the quadratic optimization method (Wu et al., 2003). The posterior class probabilities were employed as the mass functions for decision-level fusion.

RF classifier has also been successfully employed in applications of classification using multi-source remote sensing data (Dalponte et al., 2012; Hansch & Hellwich, 2020; Hartling et al., 2019, 2021; Y. Wu & Zhang, 2020). RF is an ensemble classifier combing a multitude of decision trees constructed at the training stage and outputs the class with a majority votes of predictions among individual decision trees (Breiman, 2001). RF establishes a number of uncorrelated decision trees by randomly selecting subsets of samples and features to reduce the risk of overfitting. RF creates a new dataset by randomly down-sampling from the original data with replacement given a training dataset. The OOB samples accounting for 1/3 of the samples from the new dataset are reserved to determine the unbiased estimate of the classification error. As discussed in section 2.3, RF can provide feature rankings based on their importance scores, determined during the OOB error calculation phase based on the MDA. RF outputs the probability values of each sample, measuring the probability of being classified to each tree species of interest. They are computed based on the proportion of decision trees predicting a given sample as a specific class.

2.4.2 Fusion Approaches to Individual Tree Species Classification

A variety of data fusion techniques in remote sensing have been developed over the last several decades to utilize multi-source data (Alonzo et al., 2014; Aval et al., 2019; Chang & Bai, 2018; Dalponte et al., 2012; Fassnacht et al., 2016; Ghassemian, 2016; Hu

et al., 2021; Joshi et al., 2016; Pohl & Van Genderen, 1998; Zhang, 2010). Fusion approaches aim to improve classification performance by utilizing multi-source remotely sensed data that contribute complementarily to distinguishing tree species. It can be typically grouped into three categories: pixel-level fusion (data fusion), feature-level fusion, and decision-level fusion (Pohl & Van Genderen, 1998). Remote sensing data over the same scene are commonly combined into a new dataset after geometric registration at pixel-level, such as pan-sharpening methods applied to MSI (Ghassemian, 2016). Fusion at either feature or decision level is commonly used in classification and thus is the focus of this study.

Feature-level fusion aggregates features from the respective data sources into a single feature vector for subsequent classification (Ghassemian, 2016). Feature-level fusion highlights complementary features from multiple sensors measuring different physical properties of trees, which provides a more comprehensive description of tree crowns. Feature fusion can achieve the joint optimization of the rich feature space from multi-source data. However, the high dimensionality in the feature space is likely to be a concern for applications where the size of training samples is small (Maxwell et al., 2018). The fusion process at the feature level requires extracting distinctive features of objects from the input images prior to the fusion scheme combining various features. A more informative feature space is created to identify targets of interest from a heterogeneous environment by fusing these features. Chang and Bai (2018) also pointed out that the core of the fusion approach at the feature level is the accurate selection and extraction of features from multi-source data. Diversified features could complicate the critical characteristics of

the target of interest, and inaccurate feature extraction may result in an inaccurate fusion outcome (Chang & Bai, 2018).

Most of the related studies on tree species classification were performed at the feature level. For example, Hartling et al. (2019) employed a feature-level fusion approach classifying eight dominant tree species in St. Louis, MO, USA, using WV-2 VNIR, Worldview-3 SWIR, and LiDAR intensity image and achieved the best overall accuracy of 82.6% with deep learning classifier. Unlike Hartling et al. (2019), Alonzo et al. (2014) fused hyperspectral imagery and LiDAR data at the feature level by combining spectral features and structure features to classify 29 common tree species in Santa Barbara, California, USA, with a Canonical discriminant analysis classifier. Notably, they achieved an overall accuracy of 85.4% for 725 manually delineated tree crowns. Almost all of these studies have demonstrated that combining complementary features derived from optical imagery and LiDAR data significantly improved the classification accuracies compared with single dataset-based classification.

In contrast to feature-level fusion, a decision-level fusion approach merges the preliminary classification results from several independent data sources following proposed decision rules to obtain a final result (Schmitt & Zhu, 2016). Decision fusion can effectively handle high-dimension by integrating multiple classifiers with relatively small feature sizes. Furthermore, fusion approach at the decision level can flexibly improve the generalization performance of classification instead of relying on a single classification result (Chang & Bai, 2018). Each data source is analyzed separately at the decision fusion stage, and the uncertainty and imprecision associated with each data source can be

measured and considered in the fusion process. As a result, the decision-level fusion can measure the uncertainties inherited from independent data sources based on the degrees of confidence or scores (Schmitt & Zhu, 2016). Several studies focused on the decision-level fusion in the literature. For instance, Stavrakoudis et al. (2014) employed a decision fusion approach to mapping pixel-based tree species in Macedonian forest by combining the respective independent fuzzy classification results from hyperspectral and MSI. The proposed decision fusion scheme reached an overall accuracy of 78.9%, increasing MSI-based classification by 8% and hyperspectral imagery by 12%.

The commonly used decision fusion approaches are based on fuzzy and possibility theory, voting methods, and statistics. Among them, the Dempster-Shafer theory (DST) (Dempster, 1968; Shafer, 1976) is simple yet effective, and it integrates complementary features derived from different data sources and their uncertainties for tree species classification. DST was initially introduced as a mathematical theory of evidence based on belief functions and plausible reasoning and has been widely used to combine separate pieces of information (evidence) from different sources to calculate the synthetic probability of an event.

A fusion approach utilizing the combination rules of DST evidence inference provides the possibility of performing individual data sources in their native properties and makes the multi-source data processing easy to implement. However, challenges remain in utilizing DST to qualify multi-source information, for instance, how to determine the Basic Probability Assignment (BPA) from individual datasets. With machine learning techniques, such as SVM and RF, the multi-class posterior probabilities could be calculated to establish

BPA in the frame of the DST combination rule of evidence.

The frame of discernment, denoted by θ, is firstly defined in DST, which contains all the possible classes A_i under consideration. When $\theta = \{A_1, A_2 \dots A_i\}$, the power set 2^θ contains all the subsets A_i of θ (denoted as $A_i \subseteq 2^\theta$), including the empty and full sets. DST uses a mass functions $m(A_i)$, also called BPA or basic belief assignment (BBA), to represent the degree of belief in classes given the relevant and available evidence that supports the claim that the actual class belongs to A_i . In this study, the mass function $m(A_i)$ is in the form of probabilities. For any $A_i \subseteq 2^\theta$, $m(A_i) \in [0,1], m(\emptyset) = 0,$ and $\sum_{A_i \subseteq 2^\theta} m(A_i) = 1.$

In this study, more than one set of evidence is available, and the decision to classify tree species is made based on the accumulation of all the evidence. DST allows combining the class probabilities resulting from multi-source remote sensing data and arrives at a degree of confidence taking into account all the available evidence for making the final decision. Dempster's rule of combination (the joint mass) aggregates multiple mass functions calculated from pieces of evidence (here, preliminary classification results as posterior probabilities from respective MSI, PAN, and LiDAR data). The most common decision rule defined by Shafer (1976) (Eq. 2-6) is applied to combine multi-source remotely sensed data for tree species classification in this study. The decision criterion that the maximum probability indicates the most credible or plausible decision is used in the current study to ultimately classify a given sample into one of the interested tree species classes.

$$\begin{cases} m_{1,2,\dots,i}(A) = \frac{\sum_{B_1 \cap \dots \cap B_n = A} \prod_{i=1}^{n} m_i(B_i)}{1-\mathrm{K}} \\ K = \sum_{B_1 \cap \dots \cap B_i = \emptyset} \prod_{i=1}^{n} m_i(B_i) \end{cases} \quad (2\text{-}6)$$

2.4.3 Classification Accuracy Assessment

The performance of classification methods is commonly assessed by comparing the predicted results with ground truth data in an independent test set. The confusion matrix is a standard means of evaluating classification accuracy, based on which the overall accuracy, kappa coefficient, and F1-score can be calculated (Stehman, 1997). The confusion matrix is a cross-table with columns containing actual classes and the rows with predicted classes. The overall accuracy is the proportion of correct predictions to the total number of predictions. Moreover, the kappa coefficient is a statistical measure of the agreement between the ground truth and predicted classes, considering the possibility of the agreement occurring by chance. It evaluates the classification performance in comparison with randomly assigning values. The following function defines the kappa coefficient:

$$Kappa = \frac{p_o - p_e}{1 - p_e} \quad (2\text{-}7)$$

where p_o is the overall accuracy (the proportion of classes in agreement among predictions), and p_e is the possibility of classes in agreement occurring by chance. Landis and Koch (1977) provided a scheme to interpret the value of the kappa coefficient, in which a value < 0 indicated no agreement, 0–0.20 as slight, 0.21–0.40 as fair, 0.41–0.60 as moderate, 0.61–0.80 as substantial, and 0.81–1 as almost perfect agreement.

The F1-score is a harmonic mean of the user's accuracy and producer's accuracy,

combining the two performances into a single measure that expresses both properties. F1-score ranges from 0 to 1, among which the highest possible value of 1 indicates perfect results of both user's accuracy and producer's accuracy. User's accuracy is the fraction of correctly identified samples among all the samples classified into this class, indicating the probability that prediction represent reality. Whereas producer's accuracy is the ratio of the correctly classified samples to the ground-truth samples in each class, indicating the quality of the classification of training set.

Chapter 3

Study Area and Data Processing

3.1 Study Area

The study was conducted using data covering the Keele Campus of York University located in the Greater Toronto Area, Ontario, Canada (43.77° N, 79.50° W), with 457 acres of land to present an urban environment for tree species classification (Figure 3-1). A wide variety of tree species are available in this area. The dominant tree species for the deciduous are Norway maple (*Acer platanoides)* and honey locust (*Gleditsia triacanthos)*, while the dominant tree species for the coniferous are Austrian pine (*Pinus nigra)*, white spruce (*Picea glauca*) and Blue spruce (*Picea pungens*). As a result, these five major tree species: Norway maple, honey locust, Austrian pine, white spruce, and blue spruce, were selected in this study. Aerial imagery obtained in 2016 was also used as a visual reference image to identify trees and double-check the selected reference samples, a commentary on routine field works.

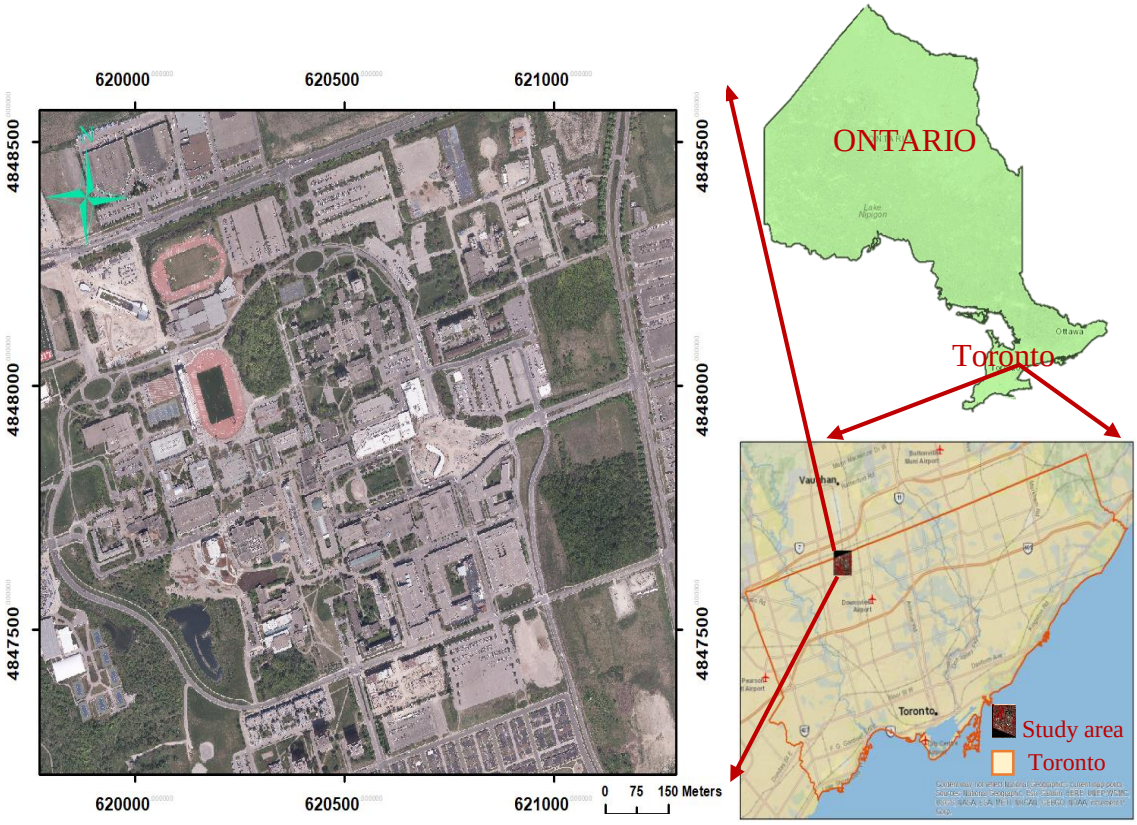

Figure 3-1 The true-colour composite of an aerial image acquired in May 2016 over the study area of Keele campus of York University located in Toronto, Ontario, Canada.

3.2 Data Used

Remotely sensed data used in this study included the WorldView-2 (WV-2) (DigitalGlobe Inc.) 8-band MSI, PAN, and airborne LiDAR data (Airborne Imaging Inc.). The specifications of WV-2 and LiDAR data are summarized in Table 3-1. The WV-2 imagery and LiDAR data were provided by the York University Map Library. A false-color composite image of the MSI and the PAN of the study area are shown in Figure 3-2.

The LiDAR data was acquired in April 2015 in early spring leaf-off conditions using a Leica ALS70-HP discrete return LiDAR system mounted on an aircraft flying at

160 knots (82.3 m/s). LiDAR data was acquired at an altitude of 800m AGL (Above Ground Level) with the laser pulse rate set at 300,000 Hz, resulting in four discrete returns and an aggregate point density of 10 points per square meter. The horizontal and vertical accuracies of LiDAR data were 30 cm and 10 cm, respectively. The 3D perspective view of the LiDAR point cloud is presented in Figure 3-3.

Table 3-1 Remotely sensed data utilized in this study.

	WV-2 MSI	**WV-2 PAN**	**LiDAR (Point cloud data)**
Data acquisition	21 July 2016	21 July 2016	11 April 2015
Spatial Resolution	1.6 m	0.4 m	10 pts/m^2 (Average density)
Spectral resolution	Band 1: Coastal (400 - 450 nm) Band 2: Blue (450 - 510 nm) Band 3: Green (510 - 580 nm) Band 4: Yellow (585 - 625 nm) Band 5: Red (630 - 690 nm) Band 6: Red Edge (705 - 745 nm) Band 7: Near-IR1 (770 - 895 nm) Band 8: Near-IR2 (860 - 1040 nm)	450 - 800 nm	Discrete 4 returns
Radiometric Resolution	16 bits per pixel	16 bits per pixel	NA

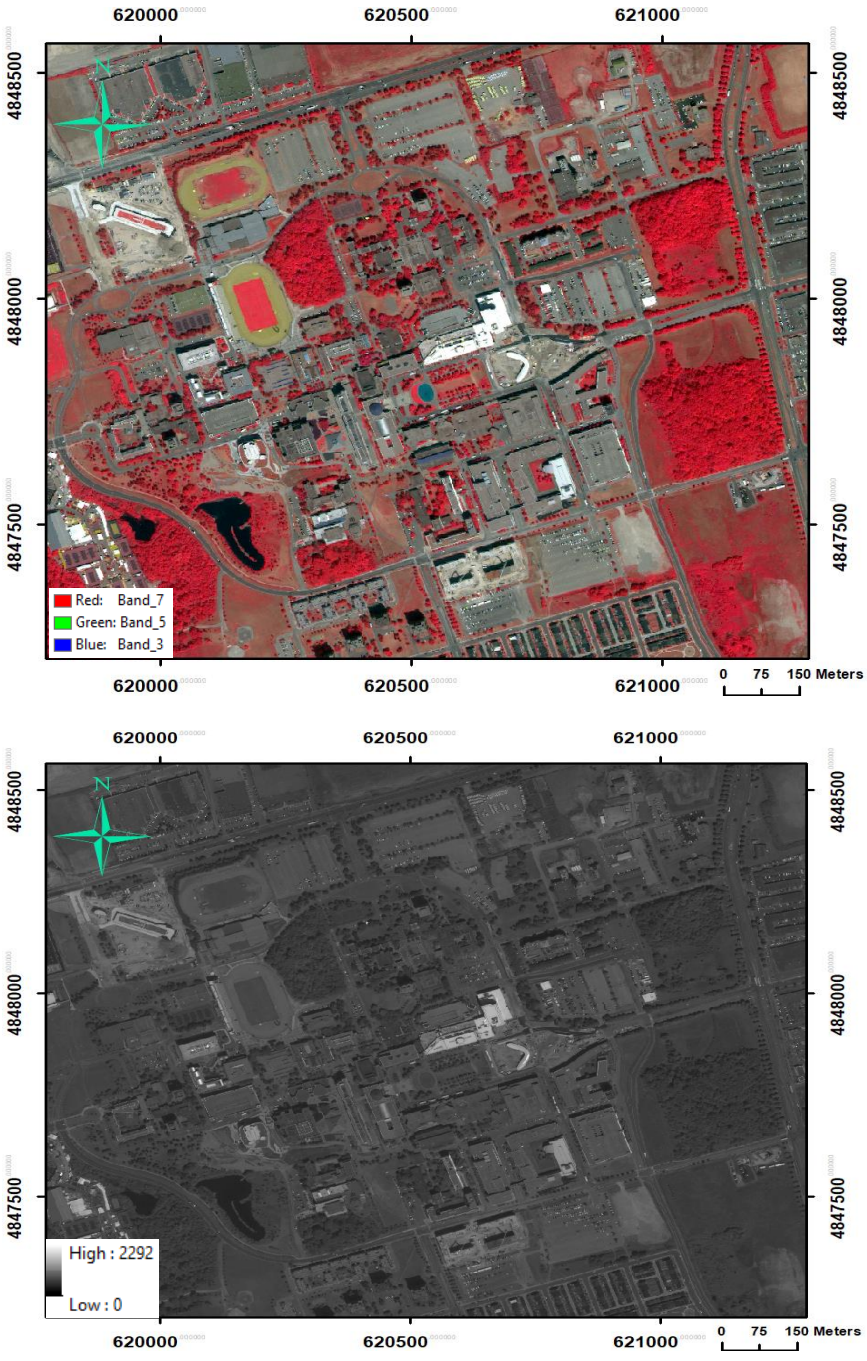

Figure 3-2 Top: a false-colour composite of the MSI with Band 7 printed as Red, Band 5 as Green, and Band 3 as Blue. Bottom: a PAN image.

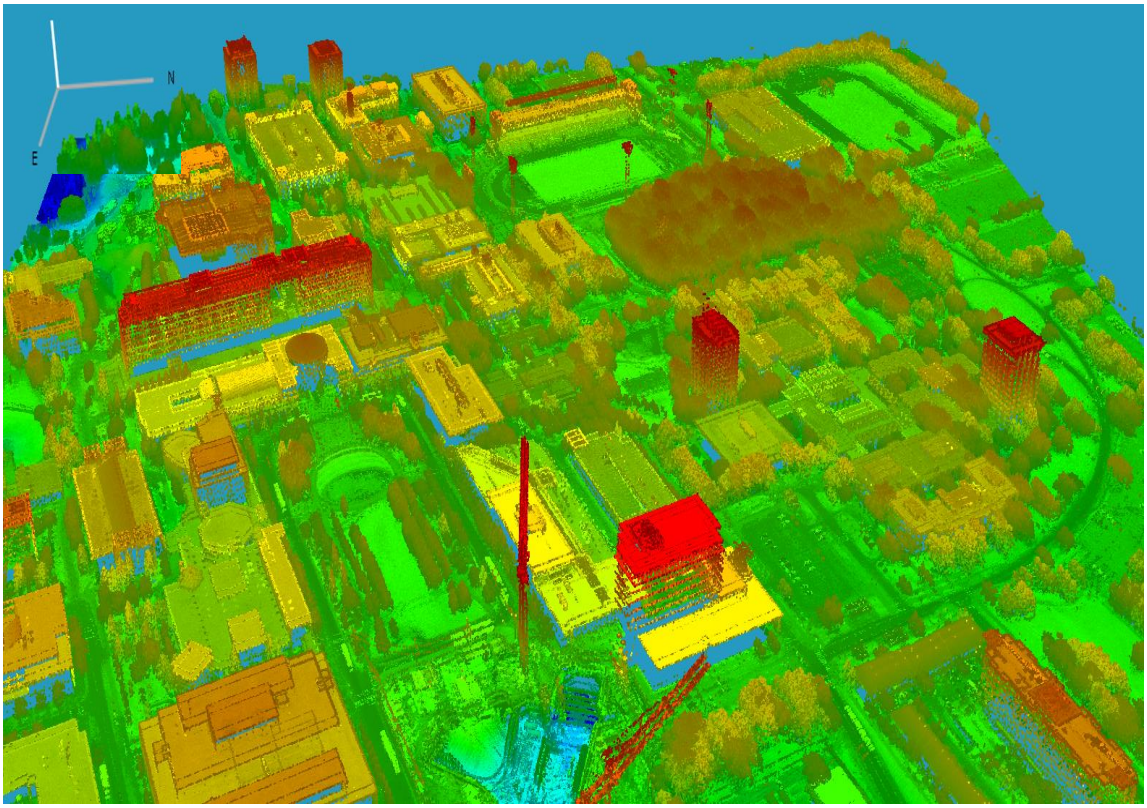

Figure 3-3 3D perspective view of the LiDAR point cloud data of the study area.

A reference sample dataset of 751 tree crowns (Table 3-2) was selected based on the pervasiveness of tree species in the street tree inventory conducted by Campus Services and Business Operations (CSBO) of York University in June 2015. The inventory map surveyed more than 5000 trees with their attributes, including tree species, location, crown size, height, and the diameter at breast height. The samples were manually delineated on WV-2 multispectral imagery using ArcMap (ArcMap 10.6), referring to individual tree crowns in the LiDAR-derived canopy height model (CHM) and the street tree inventory map. Tree species were confirmed by visually examining an aerial image acquired in May 2016 (with a spatial resolution of 8 cm by 8 cm) provided by the York University Map

Library and Google street view images under the leaf-on condition. The selected tree samples were located along streets, near buildings, and other high pedestrian areas, representing the typical distribution of trees in an urban environment. The tree samples of each species were randomly divided into training and testing subsets as a ratio of 7/3, resulting in 528 samples for training and 223 for validation. The delineated individual tree crowns were superimposed to the multi-source remotely sensed data to extract target features and create the classification sample dataset. Figure 3-4 presents an example of the delineated individual tree crowns on the PAN image, false-color MSI, and CHM.

Table 3-2 Ground reference dataset for tree species classification.

Common name	Scientific name	Tree Type	Samples Number	Proportion (%)
Norway Maple	*Acer platanoides*	Broadleaf	188	25
Honey Locust	*Gleditsia triacanthos*	Broadleaf	180	24
Austrian Pine	*Pinus nigra*	Conifer	159	21
Blue Spruce	*Picea pungens*	Conifer	115	15
White Spruce	*Picea glauca*	Conifer	109	15
		Total:	751	100

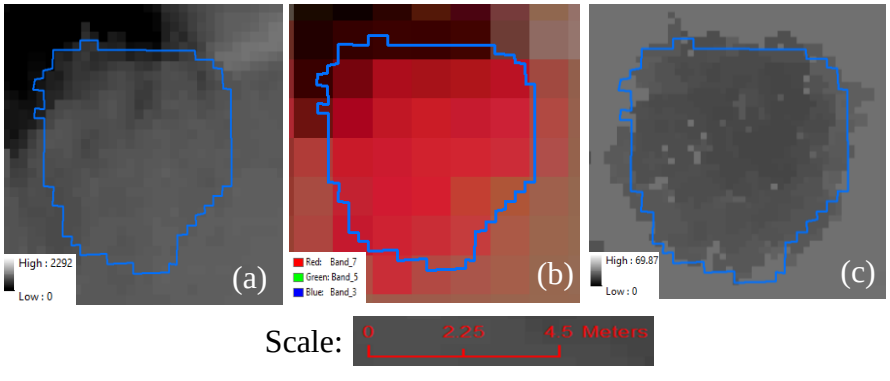

Figure 3-4 An example of a Norway maple tree crown manually delineated on (a) PAN, (b) false-color MSI, and (c) LiDAR-derived CHM.

3.3 Data Processing

The MSI was projected to the "WGS_1984_UTM_Zone_17N" coordinate system using ArcMap 10.6. It was radiometrically corrected from digital number to at-sensor radiance L based on radiometric calibration parameters and standard correction Eq. (3-1) from the WV-2 image calibration file using *MATLAB* (Version 2020a) (The Math Works, Inc., 2020).

$$L = GAIN * DN * (\frac{abscalfactor}{effectivebandwith}) + OFFSET \quad (3\text{-}1)$$

where *abscalfactor* and *effectiveBandwidth* were delivered with the imagery; The DN was the pixel value in the imagery; *Gain* and *Offset* were the absolute radiometric calibration band-dependent adjustment factors given in the file. The at-sensor radiance was converted to at-sensor reflectance using Eq. (3-2).

$$\rho_{\lambda_{Pixel,Band}} = \frac{L_{\lambda_{Pixel,Band}} * d_{ES}^2 * \pi}{E_{sun_{\lambda_{Pixel,Band}}} * \cos(\theta_S)} \quad (3\text{-}2)$$

where L was at-sensor radiance calculated independently for a defined pixel and band; d_{ES} was the Earth-Sun distance in astronomical units for the viewing day and time; E_{sun} was the band-averaged solar exoatmospheric irradiance; and θ_s was the solar zenith angle. Atmospheric correction was then carried out to obtain surface reflectance that ranges on a scale from 0 to 100% using the Atmospheric & Topographic Correction (ATCOR) model in PCI Geomatics software (PCI Geomatics 2018).

LiDAR data was processed to create a digital elevation model (DEM) and digital surface model (DSM) using the last and first returns, respectively, in MATLAB (Version 2020a) (The Math Works, Inc., 2020). The CHM, also known as the normalized digital

surface model (nDSM), was obtained as the difference between DSM and DEM. CHM was constructed at the spatial resolution of 0.4m by 0.4m, the same as the PAN. The LiDAR-derived CHM is shown in Figure 3-5.

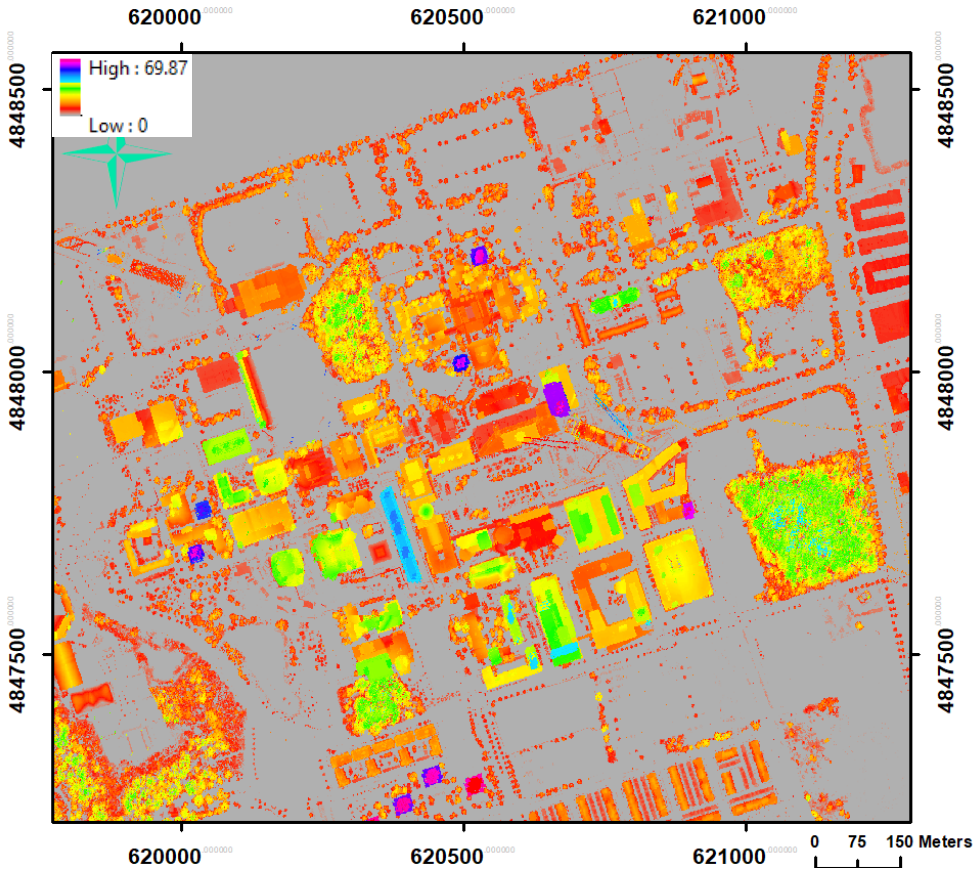

Figure 3-5 LiDAR-derived CHM of the study area.

Misalignments often exist between multi-source remotely sensed data because the accuracy of geo-referencing varies from one to the other. Accurate co-registration of optical imagery and LiDAR-derived data is crucial to using these data together. The orthorectification model using rational polynomial coefficients (RPCs) in ENVI (Harris Geospatial Solutions, Inc., 2019) was applied to align the georeferenced airborne LiDAR

data with the PAN and MSI. Ground Control Points (GCPs) were manually created to mark the prominent land features (e.g., road and path junctions, landmarks, etc.) on the PAN, whereas 3D ground control points were selected on the ground and in the air using LiDAR intensity image and DSM. They were adequate and evenly distributed across the study area. The LiDAR-derived intensity image was employed as the orthorectified reference image to align the PAN using the RPC orthorectification workflow in ENVI. This was an interactive approach to measuring errors of individual GCPs, and the overall model accuracy could be assessed. The proposed co-registration method was effective and resulted in a precise root mean square error (RMSE) of the RPCs by remaining accurate tie points after excluding the outliers, where the initial misalignment of the co-registration is improved from 18.84 pixels with 400 tie points to 0.57 pixel with 14 tie points at the resolution of 0.4 m. The co-registration method ensured corresponding pixels represent the same tree crowns by geometrically aligning images and eliminating displacement caused by differences in image acquisition time and satellite observation angle. The orthorectified PAN and LiDAR-derived DSM are shown in Figure 3-6.

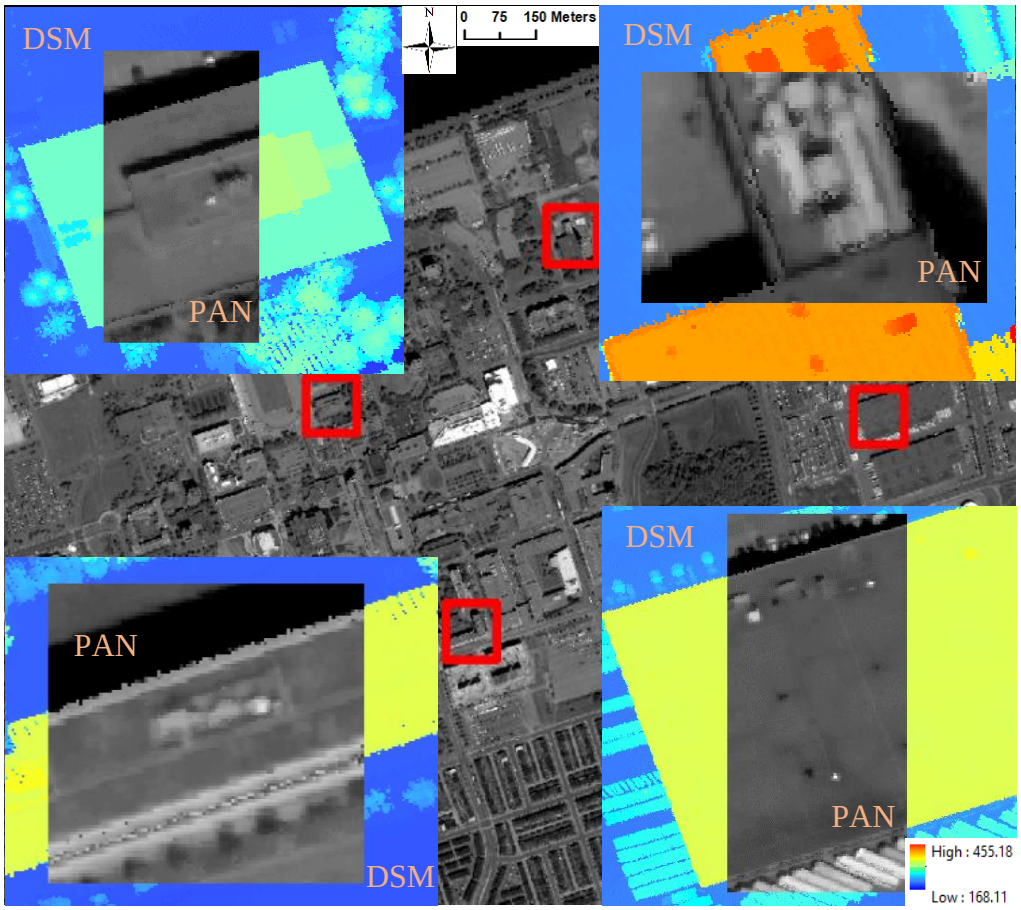

PAN in red squares scale: 0 5 10 Meters DSM scale: 0 5 10 Meters

Figure 3-6 The orthorectified PAN and DSM using the proposed co-registration method. Areas in red squares are examples of four areas to shown the co-registration result.

Chapter 4

Methodology

Spectral, textural, and structural features for individual tree crowns were derived from MSI, PAN, and LiDAR data, respectively. With these features, the following investigations were carried out:

1) The classification was performed with spectral, textural, and structural features individually to determine their discriminant power in separating five tree species of interest. In addition, the contributions of advanced textual and structural features were also explored.
2) Classification using feature-level fusion was carried out. All possible combinations of individual spectral, textural, and structural feature groups at feature-level fusion were investigated and compared to enhance the understanding of the performances of different classification schemes using the feature fusion approach. Table 4-8 summarizes all the designed feature fusion schemes.
3) Decision-fusion classification was performed, and an in-depth analysis was conducted.

In subsequent paragraphs, features extraction, feature selection, and classification methods (in general) are described in Sections 4.1, 4.2, and 4.3, followed by the presentations and the three investigations mentioned above.

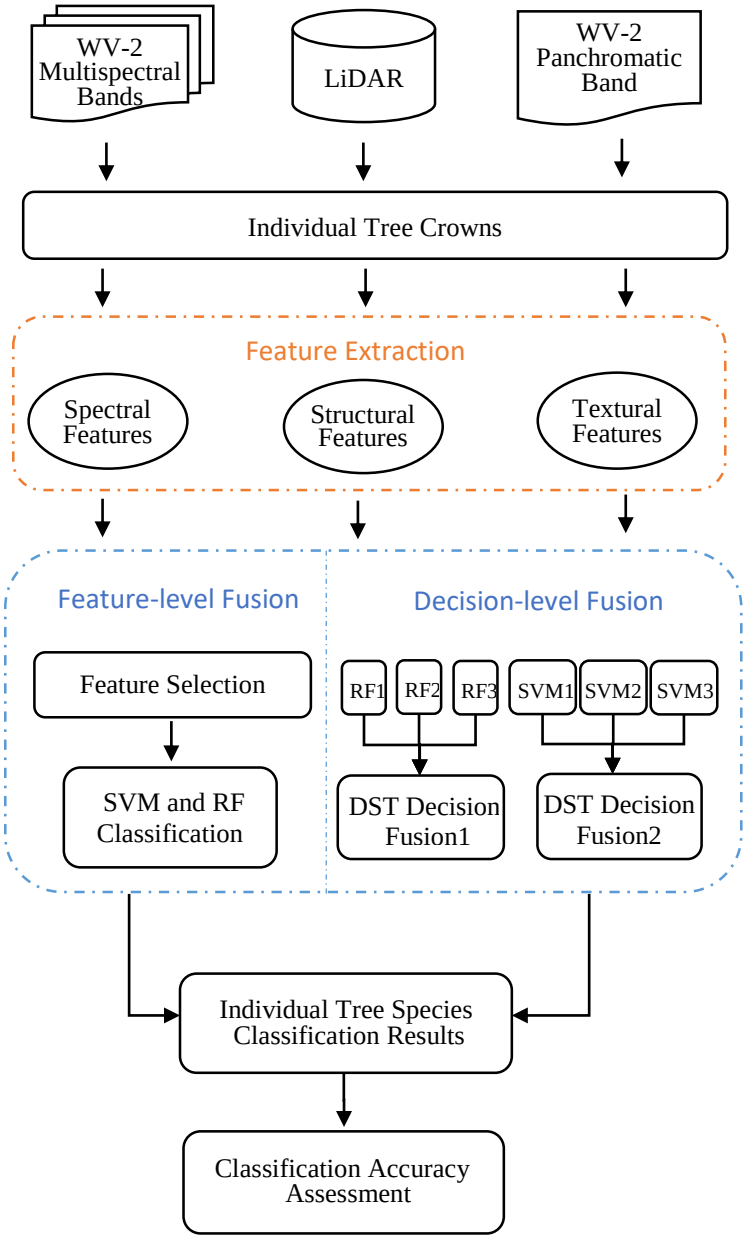

Figure 4-1 Workflow of proposed object-based tree species classification.

4.1 Feature Extraction

Information on the physical and biophysical characteristics of the five species was collected and shown in Table 4-1 to aid the extraction of suitable features for the

classification of tree species of interest. These characteristics can be represented by spectral, textural, and structural information exhibited in remotely sensed data, as displayed in Table 4-2. Tree species and their scientific names and the ground truth photo of an example of each tree species are presented in the first two columns of Table 4-2. The spectral curves of the tree crowns derived from MSI, PAN image, and LiDAR points cloud data were shown in the third, fourth, and last columns, respectively, in Table 4-2. Based on the characteristics of individual tree crowns shown in Tables 4-1 and 4-2, three feature categories were derived for species classification, as described in the following sections.

Table 4-1 The biophysical characteristics of five tree species of interest.

Species of Interest	**Leaf and color**	**Crown**
Norway Maple	Opposite, 5-lobed, coarsely toothed, and pointed leaf, dark green, large but typically wider than long	Round or oval-shaped; crown with sparse, dark holes
Honey Locust	Pinnately compound leaf bright green, but yellowish gold by fall	Wide canopy, flat-topped crown, spreading shaped with angular branches, dense clusters, fuzzy/airy crown
Austrian Pine	Simple needle-like parallel leaf, dark green	Tall columnar shaped, coarse, patchy, prominent
Blue Spruce	Stiff and sharp needles attached individually and evenly to branches, blue-green color	Pyramidal or Conical shaped, dense crown
White Spruce	Short, stiff, 4-sided needles point in every direction; bluish-green or green in color, with a whitish powdery, waxy layer	In open grows conical, spire-like crown, with a rounded top; self-pruning in dense stands branches, coarser branching

Table 4-2 Ground photos and corresponding spectral signature and representation in PAN and LiDAR data of example tree crowns delineated manually for the five species of interest.

Species (*scientific name*)	Ground Photos	Spectral Curve	PAN Image	3D plots of LiDAR Points data
Norway Maple (*Acer platanoides*)		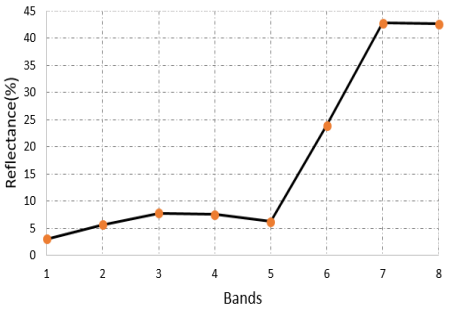	Scale:  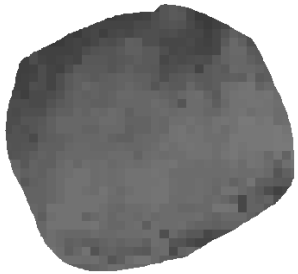	
Honey Locust (*Gleditsia triacanthos*)	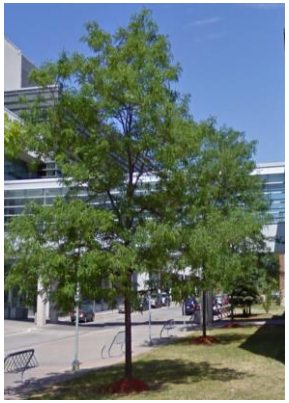	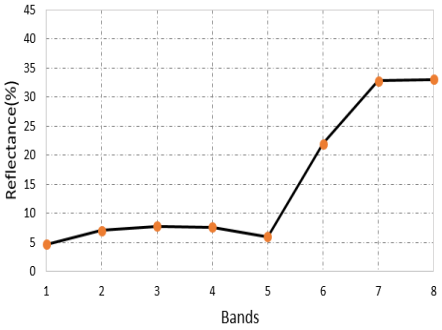	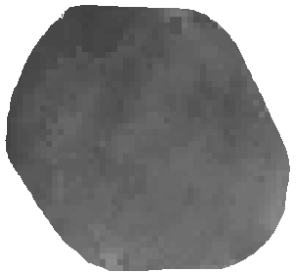	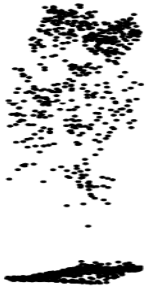

Austrian Pine
(*Pinus nigra*)

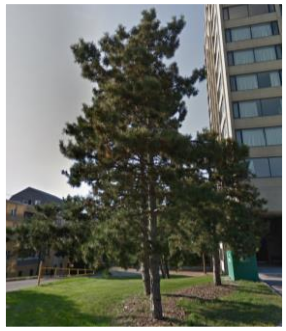

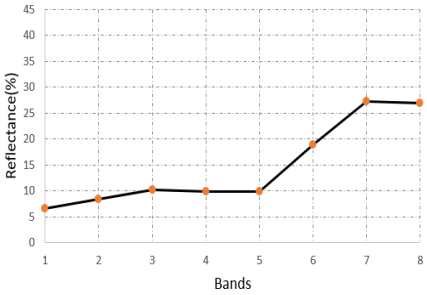

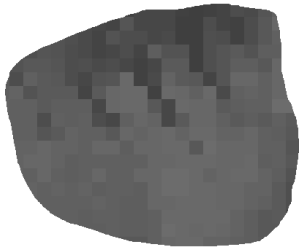

Blue Spruce
(*Picea pungens*)

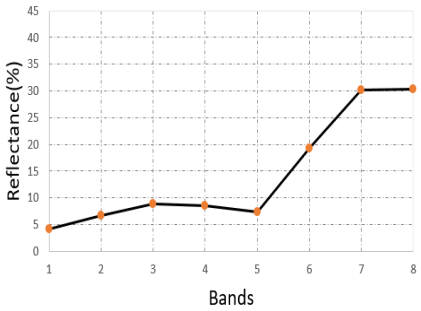

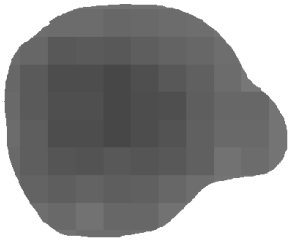

White Spruce
(Picea glauca)

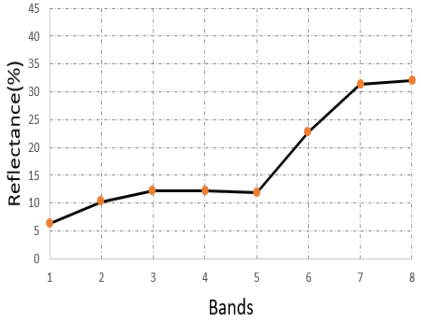

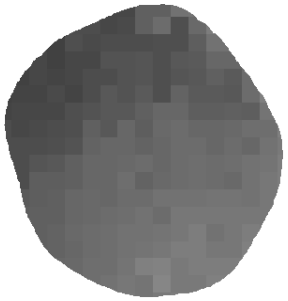

4.1.1 Spectral Features Derived from MSI

Different species may have different biochemical and biophysical properties, leading to the difference in reflectance. This mainly drives the use of spectral signatures in tree species classification. Based on previous research in the literature, the following spectral features were extracted from WV-2 MSI to evaluate the performance of spectral signatures in distinguishing tree species, including the mean and standard deviation of the reflectance of individual tree crowns at each spectral band (16 in total), and five vegetation indices consisting of NDVI, GNDVI, RNDVI, EVI, and OSAVI. Detailed descriptions of the extracted spectral features are summarized in Table 4-3.

Table 4-3 Spectral features utilized for tree species classification (16 statistic spectral features and five vegetation indices). ρ_{NIR1} refers to reflectance in Near Infrared band-1, ρ_{Red} refers to reflectance in red band, ρ_{Blue} refers to reflectance in blue band, ρ_{Green} refers to reflectance in green band and $\rho_{RedEdge}$ refers to reflectance in RedEdge band of WV-2 satellite.

Feature (Abbreviation)	Description	Reference
SpecMean	Average reflectance value of pixels within a single tree crown in each spectral band	
SpecStd	Standard deviation of the reflectance value among a single tree crown in each spectral band	
Normalized Difference Vegetation Index (NDVI)	$(\rho_{NIR1} - \rho_{Red})/(\rho_{NIR1} + \rho_{Red})$	(Rouse et al., 1974)
Green Normalized Difference Vegetation Index (GNDVI)	$(\rho_{NIR1} - \rho_{Green})/(\rho_{NIR1} + \rho_{Green})$	(Gitelson & Merzlyak, 1994)
Red Edge Normalized Difference Vegetation Index (RENDVI)	$(\rho_{RedEdge} - \rho_{Red})/(\rho_{RedEdge} + \rho_{Red})$	(Gitelson & Merzlyak, 1994)
Optimized Soil Adjusted Vegetation Index (OSAVI)	$\frac{(1 + 0.16)(\rho_{NIR1} - \rho_{Red})}{(\rho_{NIR1} + \rho_{Red} + 0.16)}$	(Rondeaux et al., 1996; Wu et al., 2014)
The enhanced vegetation index (EVI)	$2.5 * (\rho_{NIR1} - \rho_{RED})/(\rho_{NIR1} + 6 * \rho_{Red} - 7.5 * \rho_{Blue} + 1)$	(Huete et al., 2002)

4.1.2 Textural Features Derived from High-Resolution PAN

As shown in the fourth column of Table 4-2, high spatial resolution PAN from WV-2 exhibits significant potential to characterize individual tree crowns of different species. PAN was used due to its high spatial resolution (0.4 m). One might argue that if MSI were used, more information might be revealed. However, the spatial resolution of WV-2 MSI was much lower (1.6 m) compared with PAN and thus there were not many pixels within individual tree crowns to show meaningful textures. In this study, a set of textural features based on statistical GLCM texture analysis and Gabor filter technique was derived from PAN.

Twenty-two statistical GLCM texture measures were generated as a function of the co-occurring values of neighboring pixel pairs from multiple GLCMs calculated from each tree crown. The GLCM feature set in the current study was expanded from the original Haralicks' textural features. GLCMs were created at an array of offset parameters defining pixels' spatial relationships that specify all four directions (0°, 45°, 90°, and 135°) with a distance of one pixel and a number of 64 distinct gray-level. The one-pixel distance was chosen considering the 0.4m spatial resolution to measure the detailed spatial variations of individual tree crowns. In this case, each input tree crown is represented by GLCM vectors in four directions, then averaged out to calculate the statistical texture features. The computational process of these texture statistics was completed using *MATLAB* (Version 2020a) (The Math Works, Inc., 2020). Table 4-4 lists the description and formulas defining 22 GLCM-based textural features considered in this study. Among them, contrast, correlation1, energy, entropy, inverse difference moment, sum of squares: variance, sum

average, sum variance, sum entropy, difference variance, difference entropy, information measure of correlation1, and information measure of correlation2 were formulated by Haralick et al. (1973). Soh et al. (1999) discussed five additional features, including cluster prominence, cluster shade, dissimilarity, autocorrelation, and maximum probability. Correlation2 and homogeneity were computed following the formulas in *MATLAB* (Version 2020a). Two modified features, inverse difference normalized and inverse difference moment normalized, were indicated by Clausi (2002). Here, $p(i,j)$ is the$(i,j)^{\text{th}}$ element in a normalized symmetrical GLCM, and N be the number of distinct gray-levels in the image of a tree crown. μ_x, μ_y, σ_x and σ_y are the mean and standard deviations for the rows and columns of the matrix as defined in Eq. (4-1), (4-2), (4-3), (4-4) below. $p(i)$ is the i^{th} entry in the marginal-probability matrix obtained by summing the rows of $p(i,j)$.

$$\mu_x = \sum_{i,j} i * p(i,j) \tag{4-1}$$

$$\mu_y = \sum_{i,j} j * p(i,j) \tag{4-2}$$

$$\sigma_x = \sum_{i,j} (i - \mu_x)^2 * p(i,j) \tag{4-3}$$

$$\sigma_y = \sum_{i,j} \left(j - \mu_y\right)^2 * p(i,j) \tag{4-4}$$

Table 4-4 GLCM-based textural features utilized in this study.

Feature	Description	Formula
Energy	Measures of the number of repeated pairs. It is expected to be high if the occurrence of repeated pixel pairs is high. Also known as Uniformity, Uniformity of Energy, and Angular Second Moment. Range = [0 1]	$\sum_{i,j} p(i,j)^2$

Table 4-4 GLCM-based textural features utilized in this study.

Entropy	Measures of the randomness of a gray-level distribution. It is expected to be high if the gray levels are distributed randomly over the image	$-\sum_{i,j=0}^{N-1} p(i,j)log(p(i,j) = E_{xy}$
Dissimilarity	Measure the intensity contrast between pixels' pair over the image	$\sum_{i,j} \lvert i-j \rvert * p(i,j)$
Contrast	Measure the intensity contrast between pixels' pair over the image, also known as Variance and Inertia. It is expected to be low if the gray levels of each pixel pair are similar	$\sum_{i,j=0}^{N-1} \lvert i-j \rvert^2 \sum_{i,j=1}^{N} p(i,j)$
Inverse Difference Moment	Measures of the smoothness over the image, like homogeneity. It is high if the gray levels of the pixel pairs are similar	$\sum_{i,j=0} \frac{p(i,j)}{1+\lvert i-j \rvert^2}$
Correlation1	Measures the linear dependence of gray levels between the two pixels in the pixel's pair. High correlations result in large values. Range = [-1 1]	$\sum_{i,j=0}^{N-1} \frac{(ij)p(i,j)-\mu_x\mu_y}{\sigma_x\sigma_y}$
Correlation2		$\sum_{i,j=0}^{N-1} \frac{(i-\mu_x i)(j-\mu_y j)p(i,j)}{\sigma_x\sigma_y}$
Homogeneity	Measures of the closeness of the distribution of pixel pairs. It is high if the gray levels of the pixel pairs are similar. Range = [0 1]	$\sum_{i,j} \frac{p(i,j)}{1+\lvert i-j \rvert}$
Autocorrelation	Measures of the joint probability occurrence of the specified pixels' pair	$\sum_{i,j} (ij) * p(i,j)$
Cluster Shade	Measure of the joint bivariate skewness of the GLCM and the weights, unequal grey-level histogram	$\sum_{i,j} (i+j-\mu_x-\mu_y)^3 * p(i,j)$
Cluster Prominence	Measures of the groups of pixels that have similar gray-level values	$\sum_{i,j} (i+j-\mu_x-\mu_y)^4 * p(i,j)$
Maximum Probability	Measures of the occurrence of the most predominant pixel pair over the image. High occurrence of the most predominant pixel pair leads to a large value	$MAX\ p(i,j)$
Sum of Squares, Variance	Measures of how the distribution of gray levels spreads out. It is expected to be large if the distribution spreads out greatly.	$\sum_{i,j} (i-\mu_x)^2 p(i,j)$
Sum Average	Mean values of the gray levels in the image. It is expected to be large if the sum of the gray levels is high in the image.	$\sum_{i=2}^{2N} i p_{x+y}(i)$
Sum Variance	Measures of dispersion of the gray levels over the image	$\sum_{i=2}^{2N} (i-S_e)^2 p_{x+y}(i)$
Sum Entropy	Measures of the overall randomness of a gray-level distribution over the image	$-\sum_{i=2}^{2N} p_{x+y}(i)\log(p_{x+y}(i)) = S_e$
Difference Variance	Measures of the complexity and nature of gray-level transitions over the image	$\sum_{i=0}^{N-1} i^2 p_{x-y}(i)$
Difference Entropy	Measures of the complexity and nature of gray-level transitions over the image	$-\sum_{i=0}^{N-1} p_{x-y}(i)\log(p_{x-y}(i))$

Table 4-4 GLCM-based textural features utilized in this study.

Information Measures of Correlation1	Measures of the complexity and nature of gray-level transitions over the image	$\frac{E_{xy} - E_{xy1}}{\mathrm{Max}\{E_x - E_y\}}$
Information Measures of Correlation2	Measures of the complexity and nature of gray-level transitions over the image	$(1 - \exp[-2(E_{xy2} - E_{xy})])^{\frac{1}{2}}$
Inverse Difference Normalized	Differences between i and j can be normalized by the number of grey levels	$\sum_{i,j=0} \frac{p(i,j)}{1 + \lvert i-j \rvert / N^2}$
Inverse Difference Moment Normalized		$\sum_{i,j=0} \frac{p(i,j)}{1 + (i-j)^2 / N^2}$

Thirty Gabor filters in five scales and six orientations were employed in the current study. They were created with six orientations (0º, 30º, 60º, 90º, 120º, and 150º) and five different frequencies in each direction. The PAN image of individual tree crowns was convolved with each Gabor filter, resulting in 30 output images. Mean amplitude and square energy of pixels in each output image were computed using Eq. (2-3) and Eq. (2-4) to capture the variation of specific frequency content in specific directions. The Gabor filter-based textural features, mean amplitude and square energy, derived from the PAN image of individual tree crowns were added to a 60 feature vector in Table 4-5.

Table 4-5 Gabor filter-based textural features utilized in this study. SE refers to the square energy, and MA denotes the mean amplitude.

	0º	30º	60º	90º	120º	150º
f_1	SE_1 MA_1	SE_2 MA_2	SE_3 MA_3	SE_4 MA_4	SE_5 MA_5	SE_6 MA_6
f_2	SE_7 MA_7	SE_8 MA_8	SE_9 MA_9	SE_10 MA_10	SE_11 MA_11	SE_12 MA_12
f_3	SE_13 MA_13	SE_14 MA_14	SE_15 MA_15	SE_16 MA_16	SE_17 MA_17	SE_18 MA_18
f_4	SE_19 MA_19	SE_20 MA_20	SE_21 MA_21	SE_22 MA_22	SE_23 MA_23	SE_24 MA_24
f_5	SE_25 MA_25	SE_26 MA_26	SE_27 MA_27	SE_28 MA_28	SE_29 MA_29	SE_30 MA_30

4.1.3 Structural Features Derived from LiDAR

As shown in the last column of Table 4-2, LiDAR point cloud data reflected the natural arrangements of foliage and branching patterns of individual tree crowns. In this study, five types of 3D structural features were extracted to characterize the vertical profiles and 3D point distribution of individual tree crowns from LiDAR point cloud data and CHM. They are summarized in Table 4-66 and described in detail in subsequent paragraphs.

Table 4-6 The summary of structural features derived from LiDAR point cloud data and CHM.

Feature type	Feature notation	Description	Number
Foliage and branch density	$D_i = 1,2,\dots 10$	The proportion of LiDAR points per horizontal layer to the total number of points within an individual tree crown, considering layers along with tree height percentiles at 10% intervals	10
Vertical foliage clusters	$C_i = 1,2,\dots 10$	The ratio of crown areas in each horizontal layer to the maximum crown area of all layers along with tree height percentiles at 10% intervals	10
Gap distribution	$D_{gap}(j=1,2,3,4)$	Fractions of first, second, third, and last return pulses intercepted by individual tree-crown	4
3-D textural features	Twelve statistical texture features based on 3-D GLCM	Statistical method to describe the arrangement of leaf and branch using 3D GLCM, characterizing the spatial relationship of neighboring voxels with different LiDAR point distributions in tree crown	12
Height information	$H_{max}, H_{mean}, H_{min}, H_{std}$, $H_{max} * A, H_{max}$-H_{max}, $(H_{max}-H_{min})/H_{max}$, $(H_{max}-H_{mEAN})/H_{max}$, $\frac{H_{std}}{H_{max}}, \frac{H_{max}}{A}$	Statistic measures of the absolute height information of tree crowns and the combinations with the crown area	10

For the first group, the vertical distribution of foliage and branches of individual tree crowns was investigated by features characterizing the relative LiDAR point densities along with the vertical profile in this study, which was noted as D_i features. Individual tree segments were superimposed on LiDAR point cloud to extract 3D points for individual tree crowns. Each crown was then divided into ten equal horizontal layers according to the absolute height of tree crowns ranging from 1m above (the estimation of the crown base height) the ground to the maximum canopy height. The thickness of each layer was identical and equal to 10% of the absolute tree-crown height. $D_i(i = 1,2, \dots 10)$ was computed by summing the number of LiDAR points lying in the i^{th} layer, and normalizing each summary using the total number of LiDAR points within the tree crown. The D_i features were developed by (Reitberger et al., 2008) and utilized in many related studies (Hu et al., 2012; Lin & Hyyppä, 2016; Puttonen et al., 2010; Li et al., 2013). Considering the relatively lower point density of LiDAR data used in this study, ten layers were adopted to reveal the laser point distribution along the vertical profiles of trees.

In addition to the foliage and branch density related features mainly representing the quantity of foliage in each crown layer, vertical foliage cluster related features **(** C_i) (the second group) were employed to characterize the area of foliage and branches occupied in each layer. These types of features are valuable for separating coniferous and broadleaf trees since they have different spatial patterns. Broadleaf tree species tend to spread their canopy horizontally to gain more space for sunlight than conifers. 3D LiDAR points of each layer were first projected onto a 2D horizontal plane to generate a convex hull which was a convex polygon with a minimum area containing all the projected points.

The projected area bounded by the convex hull was computed to indicate the crown area of each specific layer. The maximum crown area within the tree crown was used to normalize the crown area of horizontal i^{th} layers and compute feature denoted by $C_i(i = 1,2, \dots 10)$.

The third feature type was extracted from four returns of the point data to describe the within-crown gaps, and they were denoted as the gap distribution. The gap distribution was typically identified as the proportion of the first and single returns of LiDAR laser pulse radiation intercepted by leaves representing tree crowns. Laser pulses emitted from a LiDAR system are reflected from the tree crown as multiple returns due to the natural structure of trees. In general, the first return detected by the LiDAR system presents the surface area of foliage of a tree. The intermediate returns are associated with internal tree structure, while the last return is usually from laser pulses penetrating gaps within the tree crown and the ground. The gap fraction is assumed to be equal to transmittance and opposite to the foliage cover fraction. Gap distribution-related features were computed by the following Eq. (4-5).

$$D_{gap}(j) = 1 - \frac{\sum_{z=z_i}^{z=max} R(j)}{R_{total}}, (j = 1,2,3,4) \quad (4\text{-}5)$$

where *R(j)* refers to the number of first and only returns, second returns, third returns and last returns within individual tree crowns, respectively. Studies have employed discrete return airborne LiDAR data to derive tree-crown structural features for various applications, such as gap fraction and leaf area index (Heiskanen et al., 2015). The foliage cover in the vertical direction was measured by summing the number of each return within a height range from the treetop down to an absolute height Z_i and normalising by the total number

of laser pulse returns. Returns lower than the absolute height of 1.5 m above ground were discarded to eliminate signals from the understory or the ground (i.e., understory vegetation, exposed soil, road, etc.).

Another type of structural feature derived from LiDAR point cloud data was based on 3D GLCM, characterizing the arrangement of tree elements, such as foliage, twigs, and branches. They were extracted by analyzing the 3D spatial arrangement of tree elements in the tree volume in the basis of the 3D point distribution inside the tree crown. Reitberger et al. (2009) proposed a similar voxel-based approach to tree-crown representation with the aim of individual tree segmentation using LiDAR data. Li et al. (2013) modified this method for tree species classification using high-density LiDAR data. Based on these studies, a 3D bounding box that completely contained a tree-crown volume was constructed based on eight corner coordinates using maximum and minimum x, y, and z coordinates values of LiDAR points falling within the tree crown segment. The 3D bounding box was partitioned into an axis-aligned and regular grid of discrete cubes named voxels to apply the idea of GLCM to characterizing the internal structure of tree crowns. The size of voxels was determined as 0.5 m^3 to optimally represent the internal structural properties of trees considering the point density of LiDAR data. The GLCM was calculated from 13 different directions in 3D space with a voxel distance ($d_x = d_y = d_z = 1$ voxel) relationship between neighboring voxels, whose values were derived from the cumulative number of LiDAR points lying in each voxel. The choice of the distance was based on the size of the voxel (0.5 m^3). The combined calculations of all 13 space directions were averaged to represent the general information about the internal foliage distribution of tree crowns. As a result,

12 GLCM-based statistical measures suggested by Haralick et al. (1973) were computed for classifying tree species. The detailed descriptions of these features are in Table 4-4.

The last group of features was based on the LiDAR-derived CHM. Absolute height-related features were computed at the individual tree crown scale to capture the general structural properties of tree species. Similar to some structural features proposed by Alonzo et al. (2014) and Aval et al. (2019), ten tree height-related features were extracted in this study. Table 4-6 summarizes the height information-related to structural features.

4.2 Feature Selection

RFE algorithm (Guyon & Elisseeff, 2003) was employed with an RF classifier to automatically select the most relevant and informative features from the original feature space in this study. The feature selection was only implemented for the classification scheme of feature-level fusion using the "caret" package with version 6.0-90 (Kuhn, 2008) in the statistical software RStudio (Version 1.2.1335) (RStudio Team, 2018).

RFE determined the optimal feature subset based on classification accuracies of all the possible feature combinations and feature importance ranking obtained from the RF classifier on the training dataset. RFE fitted the RF model with the initial feature space to rank them by importance at first and recursively eliminate the least important features afterward. RFE re-examined the ranked features using a permutation importance measure at each backward elimination step. This process was repeated iteratively until the optimum number of feature subset was obtained when the highest classification accuracy was produced. The importance of selected features was ranked and provided an understanding of the feature contribution to the classification accuracy based on MDA in RF (Breiman,

2001). The discriminatory power of original features extracted from multi-source remote sensing data was preliminarily evaluated by the RFE algorithm based on the feature importance, which indicated their contribution to the classification accuracies using the training dataset. Furthermore, the discriminatory power of the selected features was quantized in individual groups based on the classification accuracy using the testing dataset.

4.3 Classification Using Spectral, Textural, and Structural Features Individually

Spectral, textural, and structural features derived from MSI, PAN, and LiDAR data were used to classify five tree species using SVM and RF. Two cases were considered in the current study. In the first investigation (case A), SVM and RF classification were carried out on features individually, specifically spectral features (Table 4-3), textural features (Table 4-4 and Table 4-5), and structural features (Tables 4-6). The original features from each dataset were used to compute the posterior probabilities for the decision-level fusion approach and the classification accuracies for comparisons. A summary of the features used is listed in Table 4-7. For the second one (case B), feature selection was implemented first, and classification was performed based on the selected features (shown in Table 5-2) individually to calculate classification accuracies for the comparison with the feature-level fusion approach. The importance of individual feature groups was analyzed based on the results of the feature selection and their discriminatory powers in the classification accuracies evaluated in the second case B. In particular, textural features were subdivided into GLCM and Gabor filter-based features, and structural features were considered as

CHM and LiDAR point clouds derived features to further assess the discriminatory power of different feature types from the same dataset.

Table 4-7 Classification schemes (case A) using individual spectral, structural, and textural feature groups.

Features	Description	No.
Spectral	Statistic spectral features and vegetation indices in Table 4-3	21
Textural	GLCM measures in Table 4-4 and Gabor filter features in Table 4-5	82
Structural	Features derived from CHM and LiDAR point clouds data in Tables 4-6	46

The implementation of classification with SVM and RF algorithms was performed using "e1071" package with version 1.7-6 (Meyer et al., 2021) which is a package for R programming that provides functions for statistic and probabilistic algorithms and "randomForest" package (Liaw & Wiener, 2002) in the statistical software RStudio (Version 1.2.1335) (RStudio Team, 2018). The same training and testing datasets were used for training and validating the SVM and RF classification models. The numeric values of feature vectors derived from individual tree crowns were first normalized to a common scale from 0 to 1 before inputting to the classification models.

SVM algorithm classified tree species using the 'one-against-one' approach (Meyer et al., 2021). A total of ten binary SVM classifiers were built since five species classes were involved in this study. It is worthwhile to mention that four kernel types for SVM, namely linear kernel, polynomial kernel, radial basis function (RBF), and the sigmoid kernel were employed for the pretesting and comparison in the pretest phase.

Based on empirical experiments, the RBF kernel was selected in SVM classification models for the current research. The parameters, including the cost (C) and hyper-parameter (gamma) with RBF kernel SVM classifier, should be optimized using the training dataset to produce the best classification performance. However, using the default parameters appeared to achieve a classification accuracy close to what was achieved through the parameter optimization process after multiple verifications of empirical tests using separate feature groups. Therefore, in order to increase the generalizability of the classification model in front of multiple classification schemes, the default parameters (cost set as 1 and gamma as the inverse of number of features) of the RBF kernel SVM classifier were used for all the classification schemes in this study. Furthermore, the RBF kernel-based SVM classifier computed the posterior class probabilities of each tree sample belonging to the five tree species of interest as outputs instead of crisp class labels, which were employed as the mass functions in the subsequent decision-level fusion approach.

Two parameters were set up for the RF classifier: the number of classification trees (n_{tree}) and the number of features randomly sampled as candidates at each node (m_{try}). Based on the experiment conducted by Maxwell et al. (2018), a large number of n_{tree} was set to 500. m_{try} was varied across a wide set of values from 6 to 12 for optimizing as Breiman et al. (2018) suggested in the documentation of the randomForest package that the default value of m_{try} for classification was set to approximately the square root of the number of features in the training dataset. The m_{try} that delivered the minimum Out-of-Bag error was chosen to build the classification model. Ten-fold cross-validation with three repeats was performed to evaluate the Out-of-Bag error estimate using multiple m_{try} on the

training data. In RF, the final classification result was obtained by the tree species with the majority vote. The proportion of votes predicting each sample as a specific tree species was computed as the class-specific probabilities in the RF algorithm, enabling a soft decision fusion. The class probabilities measuring the confidence of classification results were output as the mass functions in the subsequent decision-level fusion approach.

4.4 Classification Using the Feature-level Fusion Approach

Feature-level fusion approach integrated spectral, textural, and structural features for the classification using SVM and RF algorithms. The RFE algorithm was implemented to select the most relevant features from the original features (shown in Tables 4-3, 4-4, 4-5, and 4-6) for the classification. As detailed in Chapter 5 (Table 5-2), 60 features were selected and contained 11 spectral, 20 textural, and 29 structural features. Based on the selected features, all possible feature-level fusion schemes in terms of the types of features used were investigated and compared to enhance the understanding of the relative importance of these features and their classification performances using the feature fusion approach. Table 4-8 summarizes all the designed feature fusion schemes. One might argue that feature selection needs to be done for each combination of features to get the best results. It is worth noting that it has been tried, and there was no significant difference from the feature selection conducted for all features combined together in the results; thus, they were not presented in this thesis.

Table 4-8 Classification schemes using feature-level fusion approach.

Features Combination	No.
Spectral and textural features	31
Spectral and structural features	40
Textural and structural features	49
All features	60

4.5 Classification Using the Decision-level Fusion Approach

The decision-level fusion approach combined the preliminary classification results from individual spectral, textural, and structural features derived from MSI, PAN, and LiDAR data through the DST combination rule (Eq. (2-6)) to obtain the final classification result. The workflow diagram in Figure 4-2 depicts the outline of the DST-based decision-level fusion approach deployed with SVM to tree species classification.

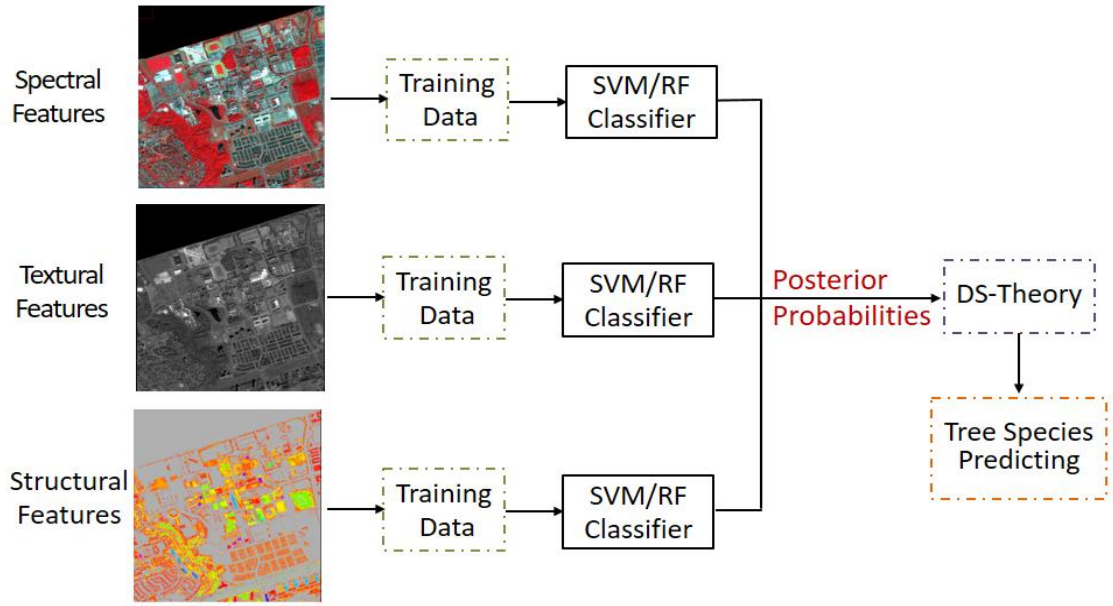

Figure 4-2 Workflow of the decision-level fusion approach deployed with SVM.

Considering the independence of data sources, individual feature groups (Table 4-3, 4-4, 4-5, 4-6) without feature selection were directly utilized to build classification models using SVM and RF algorithms, respectively, which were the same with classification schemes in Table 4-7. The classification outputs of individual feature groups were presented in the class probabilities instead of the predicted classes. The evidence or confidence of preliminary classification results from individual feature groups was quantified as numeric posterior probabilities using the improved Platt scaling method (Platt, 1999; Wu et al., 2003) in SVM and the voting of trees in RF (Breiman, 2001). For a particular tree sample, the probability indicated the percentage supporting the belief that the tree object belonged to a specific tree species. The posterior class probabilities from individual classification schemes in Table (4-7) were employed as mass functions that were further combined through the DST combination rule in Eq. (2-6) at decision-level fusion, respectively. DST-based decision fusion combined probabilities for five tree species of interest computed from multi-source features and arrived at a degree of confidence, considering all the available evidence for the decision making. The most probable tree species was ultimately assigned to a given sample based on the decision criterion of the maximum probability.

It is worth noting that the decision fusion of probabilistic SVMs and RFs was also performed in order to investigate the combination of evidence from different classification algorithms. The classification result decreased slightly in comparison with the fusion using SVMs alone. Therefore, classifications using the decision fusion approach deployed with SVM and RF were implemented and described respectively in the current thesis.

Chapter 5

Results and Discussion

5.1 Classification Using Spectral, Textural, and Structural Features Individually

As mentioned in Chapter 4, classification was performed based on spectral, textural, and structural features individually in two cases. For case A, all features were used, and feature selection was carried out prior to the classification for case B. The classification accuracies for both cases are shown in Table 5-1, and the selected features are presented in Table 5-2.

Table 5-1 Classification results of individual feature groups using SVM and RF (bold entries with the star (*) indicate the highest overall accuracy among all feature groups).

		SVM		RF	
	Feature Groups	Overall Accuracy	Kappa	Overall Accuracy	Kappa
Case A	Spectral features	0.70	0.62	0.70	0.62
	Textural features	0.76	0.70	0.75	0.68
	Structural features	0.78	0.72	0.76	0.69
Case B	Selected spectral features	0.70	0.62	0.65	0.56
	Selected textural features	0.74	0.68	0.72	0.64
	Selected structural features	**0.80***	**0.74***	**0.78***	**0.72***

In general terms, SVM and RF algorithms resulted in similar classification accuracies over all feature groups, although SVM outperformed RF slightly. The

discussion in this section focuses on the results from SVM. The results showed that spectral, textural, and structural features extracted in the current study adequately discriminated five tree species with satisfactory classification accuracy (with an overall accuracy higher than 0.7) for both cases. In addition, there was not much difference (no more than 2%) in the accuracies between using the original and selected features. Specifically, the overall accuracy based on textural features decreased by 2% after feature selection, while the selected structural features improved the overall accuracy by 2%. Nevertheless, feature selection performed well with a significant reduction in the number of features used (Table 5-2) in this study, where 60 out of 149 features were selected. The detail of the determination of the number of selected feature subsets and the importance of each selected feature are discussed in section 5.2.

Table 5-2 shows that eleven spectral features from MSI were selected from the original 21 features as informative features for tree species classification. According to the whitepaper of WV-2, these selected spectral bands such as Red Edge, NIR1, and NIR2 bands are particularly beneficial in the discrimination between types of vegetation, significantly aiding in tree classification. Not only the mean reflectance of individual tree crowns in selected spectral bands were significant, but also the standard deviation and vegetation indices were important in species classification, which were consistent with the analysis of spectral features in the literature (Clark et al., 2005; Fassnacht et al., 2016; Waser et al., 2014).

For the textural features, half of (11) 2D GLCM-based features were selected out of the 22 original features. The commonly used GLCM features were significant, such as

correlation, entropy, and information measure of correlation. However, the less employed GLCM features, such as cluster shade, cluster prominence, and inverse difference normalized, were also selected. Moreover, only nine Gabor filter-derived features were selected since the original 60 Gabor filter-based textural features were extracted. It was expected since such a large feature space was prone to the high redundancy.

For the structural features, 29 out of 44 features were selected from LiDAR point cloud data. It made sense that these structural features were selected because they provided the essential and complementary information of internal tree crowns for tree species interested from the 3D perspective, of which optical images lack. However, it must be noted that only 4 out of 12 3D GLCM-based textural features characterizing the arrangement of foliage and branch inside individual tree crowns were selected. This was probably related to the point density of the LiDAR used (10 points per m^2). With this point density, the number of LiDAR points within individual tree crowns was not significant, especially for small trees. In comparison, all 10 features from LiDAR-derived CHM were selected, which was consistent with the finding by Dalponte et al. (2012) that height-related features derived from LiDAR data with low (0.48 points per m^2) and high (8.6 points per m^2) point density performed similarly in improving the classification accuracy of hyperspectral and multispectral imagery.

Table 5-2 Selected features from MSI, PAN, and LiDAR data for tree species classification.

Dataset	Feature Group	Selected features	No.	Representatives of a single tree crown's characteristics
MSI	Spectral Features	Reflectance_B4,6,7,8; SD_B2,6,7,8	11	Mean and standard deviation of the reflectance of tree crown at band-2, band-4, band-6, band-7, band-8
		EVI, GNDVI, RE_NDVI		Combination of reflectance at different bands (EVI, GNDVI, RNDVI)
PAN	Textural Features	2D-Correlation, 2D-ClusterProminence, 2D-ClusterShade, 2D-Entropy, 2D-InverseDifferenceMoment, 2D-SumVariance, 2D-MaximumProbability, 2D-DifferenceEntropy, 2D-InformationMeasureofCorrelation1, 2D-InformationMeasureofCorrelation2, 2D-InverseDifferenceNormalized	11	2-D GLCM based texture analysis describes the variations in intensity of pixels belonging to tree crowns in PAN
		GaborFilter-SquareEnergy 1,2,17,18,21,22,24 GaborFilter-MeanAmplitude1,21	9	Gabor filter based textural features provide robustness against varying brightness and contrast of pixels within tree crown in PAN
LiDAR point clouds	Structural Features	Density_Layer1,2,3,4,5,9	6	Normalized number of points at horizontal layer-2,layer-3, layer-4 using the total number of individual tree points, presenting the branch and foliage distribution at vertical profile
		Area, Vertical_cluster1,2,5,9,10	6	Crown area and the ratio of the crown areas to the maximum crown area at horizontal layer-1, layer-2, layer-6, layer-7, layer-8, presenting the vertical foliage clusters at these layers
		Gap_distribution1, Gap_distribution2, Gap_distribution3	3	The proportion of first, second, and third returns subtracted from 1, presenting gap distribution within tree crown opposite to foliage covers
		3D-Contrast, 3D-SumMean, 3D-ClusterShade, 3D-ClusterTendency	4	Measures of the 3D spatial relationship of neighboring voxels with different LiDAR point numbers in a tree crown, characterizing the arrangement of foliage, twigs and branch
CHM		Max_H/Area, Max_H*Area, SD_H/Max_H, Mean_H, (Max_H-Min_H)/Max_H, Max_H, Mean_H, (Max_H-Mean_H)/Max_H, Max_H-Mean_H, SD_H	10	Absolute tree height statistics and the combinations with area information

The contribution of the advanced textural features and structural features were further demonstrated based on the classification accuracies shown in Table 5-3, where the F1-score and overall accuracy of selected features in groups are detailed. F1-score was involved in a comprehensive analysis of the classification contribution of feature groups on each tree species. As discussed in 4.3, GLCM and Gabor filter-based textural features and CHM and 3D LiDAR points-based features were analyzed, respectively, in Table 5-3.

Table 5-3 Classification results of case B (bold entries with the star (*) indicate the highest F1-score for each species and feature group with the highest overall accuracy).

	Norway Maple	Honey Locust	Austrian Pine	Blue Spruce	White Spruce	OA
SVM Classification						
SF	0.87	0.71	0.69	0.58	0.49	0.70
TF_GLCM	0.91	0.67	0.65	0.68	0.54	0.71
TF_GABOR	0.80	0.38	0.69	0.40	**0.60***	0.60
TF	0.89	0.70	0.74	**0.72***	0.58	0.74
STF_CHM	0.90	0.70	0.74	0.54	0.49	0.71
STF_3D	0.85	0.67	0.86	0.62	0.56	0.74
STF	**0.93***	**0.80***	**0.90***	0.67	0.53	**0.80***
RF Classification						
SF	0.88	0.69	0.65	0.46	0.35	0.65
TF_GLCM	0.88	0.67	0.62	0.60	0.46	0.67
TF_GABOR	0.82	0.33	0.63	0.42	**0.59***	0.58
TF	0.90	0.67	0.71	**0.65***	0.54	0.72
STF_CHM	0.91	0.73	0.72	0.57	0.48	0.72
STF_3D	0.88	0.70	0.82	0.61	0.53	0.74
STF	**0.93***	**0.77***	**0.86***	0.63	0.51	**0.78***

*SF: Spectral features.
TF_GLCM: Textural features based on the statistical 2D GLCM.
TF_GABOR: Textural features based on the Gabor filter method.
TF: The combination of GLCM and Gabor filter-based features.
STF_CHM: Structural features extracted from LiDAR-derived CHM.
STF_3D: Structural features extracted from 3D LiDAR point cloud data.
STF: Combined CHM and 3D structural features.

For specific tree species classifications, each feature group exhibited different discriminatory powers. With the highest F1-score for Norway maple, honey locust, and Austrian pine, the structural feature group (STF) combining CHM and 3D point cloud-based features (STF_CHM and STF_3D) was able to effectively distinguish these three tree species in comparison with other feature groups. On the other hand, TF resulted in the highest F1-score when separating blue spruce and white spruce. The main reason for this is that the natural crown cross-sectional area and crown volume of these coniferous trees affect the effective extraction of spectral features and structural features. It was worth noting that among five tree species of interest, Norway maple showed the highest classification accuracies using each feature group in Table 5-3. This mainly resulted from its physical characteristics, such as wide-spreading crown and the dense foliage in comparison with other tree species with narrow crowns or the sparse foliage. Nevertheless, narrow crowns and needle leaves of blue spruce and white spruce limit the extraction of expressive spectral and structural features, which resulted in a severe misclassification between these two tree species under the spruce genus. In related studies, LiDAR-derived structural features have also been reported to have a robust discriminatory capacity for the identification of coniferous tree species with narrow crowns, for example, features measuring the distributions of laser points along with the vertical profile (Li et al., 2013, 2015), statistical analysis of height information of laser points for individual tree crowns (Yao et al., 2012), and point density of horizontal layers at particular tree heights (Lin & Hyyppä, 2016). Nevertheless, the spectral feature group (SF) contributed moderately to the classification of coniferous and broadleaf tree species, with the F1-score and overall

accuracy ranked in the middle.

For the contribution of advanced textural and structural features, according to the overall accuracy of classification models considering all five tree species, it can be concluded that STF_3D contributed more than STF_CHM with an increase of the overall accuracy of 3%. The tree height-related features alone were not able to effectively separate the tree species of interest in the study area. Caution should be made that for some cities, different species might be planted at different times and thus the variations in height might be resulted from the difference in age, even though this was not the case for the study area. Except for the STF, STF_3D indicated the most significant discriminatory power in the classifications. On the contrary, the Gabor filter feature group (TF_GABOR) contributed the least to tree species classification. The statistical GLCM feature group (TF_GLCM) slightly improved the classification using spectral features that consisted of commonly used multispectral signatures and vegetation indices. Although the discrimination powers of TF_GLCM and TF_GABOR varied greatly on classification accuracies, the textural feature group (TF) combining them improved the overall accuracy to 0.74, which is higher than SF by 4% and comparable to STF_3D. Besides, STF_CHM exhibited similar discrimination power to statistical TF_GLCM with overall accuracies of 0.71.

5.2 Classification Using the Feature-level Fusion Approach

The results of the feature selection using the RFE algorithm are presented in Figure 5-1 and Figure 5-12. The RFE feature selection algorithm determined the number of selected feature subsets according to the repeated cross-validation classification accuracies using the training dataset. As shown in Figure 5-1, classification accuracy rises with

increases in the number of selected features and reaches a plateau when the number of features is 60. As a result, the optimal feature subset was selected with 60 features from the original 149 features.

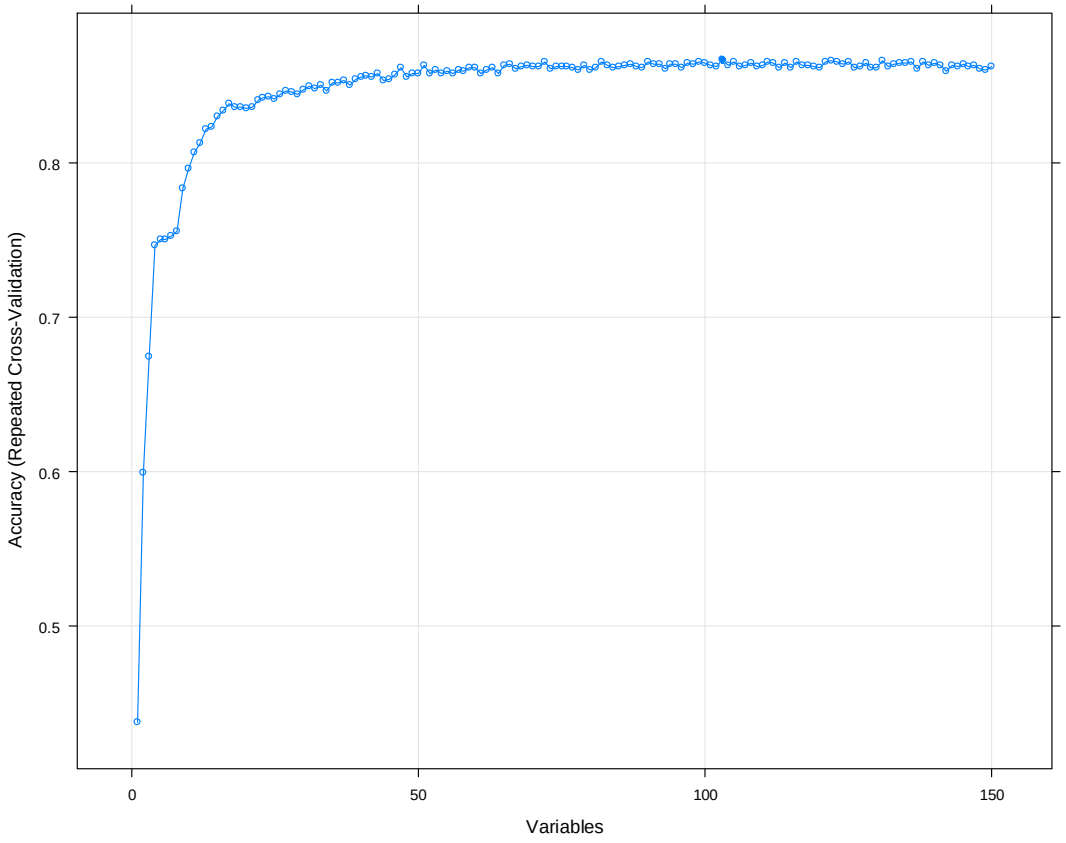

Figure 5-1 Classification accuracies versus the number of selected features using RFE.

Figure 5-2 shows the importance ranking of selected features using the RFE algorithm, ordering from the top to bottom as the most to least important features. Structural features accounted for 48 percent of the selected feature subset (60 features were selected in total). In comparison, spectral features account for 18 percent (11 features), and the proportion of textural features is 34 percent (20 features).

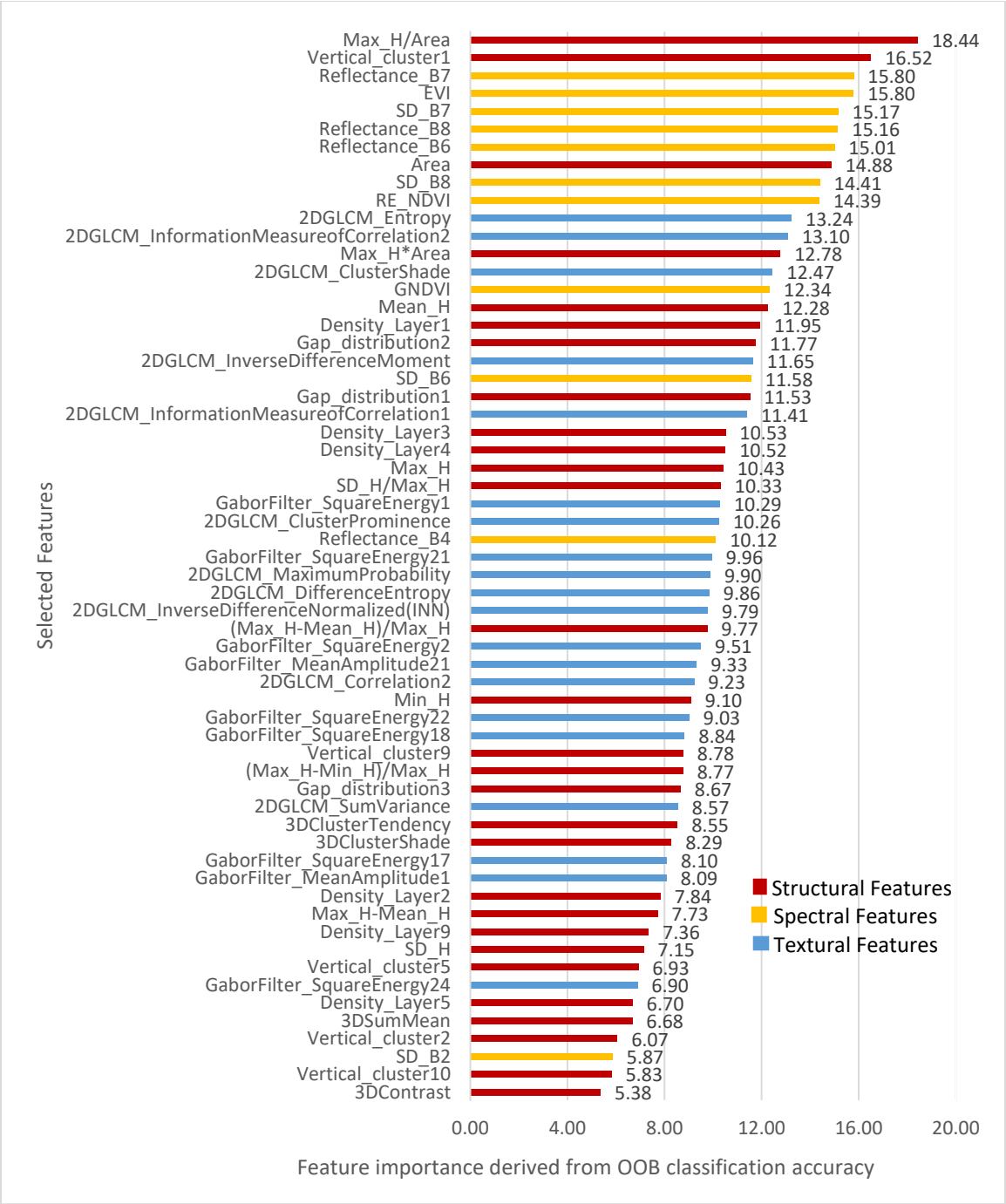

Figure 5-2 The importance ranking of selected features based on MDA in RF.

However, nine out of the top 20 most discriminative features were extracted from MSI, although the top two most discriminative features were structural features derived

from LiDAR data. The ratio of tree height and crown area placed the first in feature importance ranking, followed by the vertical cluster of foliage and branch at the treetop (the first vertical cluster). Structural features indicating crown shape, such as the ratio of crown height to the crown area, have been demonstrated to help separate tree species since they can capture inter-species variation in crown morphology (Lin & Hyyppä, 2016; Liu et al., 2017; Shi et al., 2018). Seven structural features from LiDAR CHM and point clouds data, including tree height-related statistics and 3D measures of tree elements within tree crown, were selected among the top 20 most discriminative features. On the other hand, only four textural features were ranked in the top 20 most discriminative features. They were all GLCM-based statistical measures, namely inverse difference moment, cluster shade, information measure of correlation, and entropy. Gabor filter-based features, however, tended to contribute highly redundant information. Although spectral features derived from MSI showed great importance for classification (Figure 5-2), they reached a moderate classification accuracy of 0.7 in Table 5-1.

Generally, when analyzing each feature, most of the spectral features presented the remarkable capacity to discriminate tree species, followed by structural features and textural features. In addition, reflectance information at band7- NIR1(770-895 nm), band8-NIR2 (860-1040 nm), and band6-Red Edge (705-745 nm) indicated greater discriminatory power than vegetation indices except for EVI, which is consistent with related studies (Clark et al., 2005; Fassnacht et al., 2016; Waser et al., 2014). It is worth noting that advanced structural features held the potential for increasing the discriminatory power for remote sensing-assisted tree species classification. They accounted for 48% of the final

feature subset with a wide range of importance scores. Significantly, two representative structural features with the highest importance value were placed at the top of the feature importance ranking, as shown in Figure 5-2. Features characterizing vertical cluster and density of foliage and branch at particular layers and gap distribution of tree canopies discriminated tree species more effectively than 3D GLCM-based features (e.g., 3D sum mean, 3D contrast, etc.). The importance scores of selected textural features varied widely from top to bottom, but 2D statistical GLCM-based features had higher discriminatory power than Gabor filter-based textural features according to the classification accuracies in Table 5-3.

Overall, the results and discussion on the discriminatory power of multi-source derived feature groups also demonstrated that the combination of multi-source data should be an optimal approach to improving the tree species classification accuracy since the classification accuracies using individual feature groups may not be adequate for many applications in practice. This was also verified by the feature importance ranking, which indicated that features with high importance scores for tree species classification were extracted from different feature groups and complementary. Although the LiDAR-derived structural feature group resulted in a promising overall accuracy of 0.8 using SVM, the potential for investigating the effective and efficient way to integrate the multiple feature groups confirmed the motivation of the current study of feature-level and decision-level fusion approaches.

Table 5-4 Confusion matrix for the feature-level fusion approach using SVM and RF. User's accuracy and producer's accuracy are denoted as UA and PA, respectively.

		Actual Tree Species					
	Tree Specie	Norway Maple	Honey Locust	Austrian Pine	Blue Spruce	White Spruce	UA (%)
		SVM					
Predicted Tree Species	Norway Maple	*52*	2				96.30
	Honey Locust	4	*48*	1	1	2	85.71
	Austrian Pine		2	*45*	2	1	90.00
	Blue Spruce		1	1	*26*	8	72.22
	White Spruce		1	1	6	*19*	70.37
	PA (%)	92.86	88.89	93.75	74.29	63.33	
	Overall Accuracy	85.2%					
	Kappa Coefficient	0.81					
		RF					
	Norway Maple	*51*	2				96.23
	Honey Locust	4	*45*	2	1		86.54
	Austrian Pine	1	5	*43*	1	2	82.69
	Blue Spruce			1	*26*	8	74.29
	White Spruce		2	2	7	*20*	64.52
	PA (%)	91.07	83.33	89.58	74.29	66.67	
	Overall Accuracy	82.96%					
	Kappa Coefficient	0.78					

The confusion matrix of the classification results using the feature-level fusion approach is shown in Table 5-4. The overall accuracy and kappa coefficient were 0.85 and 0.81 for the SVM classification. These values were slightly lower in RF classifications (0.83 and 0.78, respectively). In the following, the discussion is focused on SVM. According to the producer's and user's accuracies in Table 5-4, the feature fusion classification schemes led to varying performances among the five tree species. The highest producer's accuracy of 93.75% was achieved by Austrian pine, followed by Norway maple (92.86%) and honey locust (88.89%). The user's accuracies were consistent with the

producer's accuracies. The misclassification mainly occurred among blue spruce and white spruce. Seven blue spruce trees were misclassified as white spruce, while eight white spruce trees were identified as blue spruce. Tree species with wide-spreading crowns (i.e., Norway maple, honey locust, Austrian pine) were distinguished from those with narrow crowns (i.e., blue spruce and white spruce) successfully with little confusion. This result was consistent with the discriminatory power analysis on specific tree species discussed in Chapter 5.1. The misclassification between blue spruce and white spruce was mainly due to the fact that there were in the same genus and thus might exhibit similar properties in the data used in this study.

Table 5-5 Comparison of classification results at the feature-level fusion using SVM and RF (bold entries with the star (*) indicate the highest classification accuracy for classification models).

Feature Combinations	SVM		RF	
	Accuracy	Kappa	Accuracy	Kappa
Spectral + Textural	0.81	0.76	0.80	0.75
Spectral + Structural	0.83	0.78	0.81	0.76
Textural + Structural	0.82	0.77	0.81	0.76
Spectral + Textural + Structural	**0.85***	**0.81***	**0.83***	**0.78***

As mentioned in Chapter 4, classification using different combinations of features (Table 4-8) was carried out to analyze the relative contribution of each type of features in the species classification. The results are shown in Table 5-5. It was further verified that SVM and RF delivered accordant classification results. The discussion in this section

focuses on the results from SVM. Classification using the combination of spectral, textural, and structural features exhibited the best classification performance with the highest overall accuracy of 0.85 and kappa coefficient of 0.81, which outperformed the classification accuracies by using individual feature groups (Table 5-1) and using any other combination schemes in Table 5-5. Among the combinations of two types of features, classification using the spectral and structural features achieved the best result, which increased the overall accuracy of spectral features alone from 0.7 (Table 5-1) to 0.83. The most significant increase in the classification accuracies indicated that structural features significantly improved the performance of classification schemes more than other feature groups. The results in Table 5-5 demonstrated that feature fusion approaches significantly improved individual feature group-based classifications with various degrees of success. Each feature group showed a complementary contribution to the classification results when combined with different features.

5.3 Classification Using the Decision-level Fusion Approach

The confusion matrix for the classification using the spectral, textural, and structural features based on decision-level fusion is presented in Table 5-6. The overall accuracy and kappa coefficient were 85.65% and 0.82, respectively, using the SVM algorithm. RF resulted in slightly lower classification accuracies (83.86% and 0.79, respectively). Similarly, the classification results from SVM are discussed in detail. Among five tree species, Austrian pine had the highest producer's accuracy of 95.83%, showing that the most number of Austrian pine were correctly classified. Norway maple was classified with relatively high producer's accuracy (94.64%) and user's

accuracy (92.98%). The miss-classification occurred between Norway maple and honey locust. They are both deciduous and might show similar spectral, textural, or structural features. The most miss-classification occurred between white spruce and blue spruce. Nine out of 35 actual blue spruce trees were misclassified to white spruce (five), honey locust (three), and Austrian pine (one), respectively. On the other hand, ten out of 30 actual white spruce trees were misclassified to blue spruce (eight) and Austrian pine (two). It was also noted that eight honey locust trees were misclassified to Norway maple (four), Austrian pine (two), and white spruce (two), although its PA and UA were both around 85%. This was mainly due to the confusion of physical characteristics among these tree species, especially the wide-spreading crown of Norway maple, honey locust, and Austrian pine; the sparse foliage for honey locust and Austrian pine but dense one for Norway maple. Additional features, such as spectral and textural features derived from Unmanned Aerial Vehicles (UAVs) based data and structural features derived from high-density LiDAR data, are needed to effectively capture detailed tree elements, which contributes to distinguishing these easily-confused tree species mainly based on the crown spread and canopy density in the current study.

Table 5-6 Confusion matrix for the decision-level fusion approach using SVM and RF. User accuracy (UA) and producer accuracy (PA) were calculated as percentages.

		Actual Tree Species					
	Tree Specie	Norway Maple	Honey Locust	Austrian Pine	Blue Spruce	White Spruce	UA(%)
		SVM_RBF					
Predicted Tree Species	Norway Maple	*53*	4				92.98
	Honey Locust	3	*46*	2	3		85.18
	Austrian Pine		2	*46*	1	2	90.19
	Blue Spruce				*26*	8	76.47
	White Spruce		2		5	*20*	74.07
	PA(%)	94.64	85.19	95.83	74.29	66.67	
	Overall Accuracy	85.65%					
	Kappa Coefficient	0.82					
		RF					
	Norway Maple	*50*	3				94.34
	Honey Locust	5	*46*	2	1		85.19
	Austrian Pine	1	3	*46*	1	3	85.19
	Blue Spruce				*27*	9	75.00
	White Spruce		2		6	*18*	69.23
	PA(%)	89.29	85.19	95.83	77.14	60.00	
	Overall Accuracy	83.86%					
	Kappa Coefficient	0.79					

To clearly show the differences in classification accuracies of classification schemes investigated in this study, overall accuracies and kappa coefficients obtained by the classifications using spectral, textural, and structural features individually (Table 5-1) and in combination at the feature-level (Table 5-4) and decision-level (Table 5-6) fusion with SVM algorithm are compared in Figure 5-3.

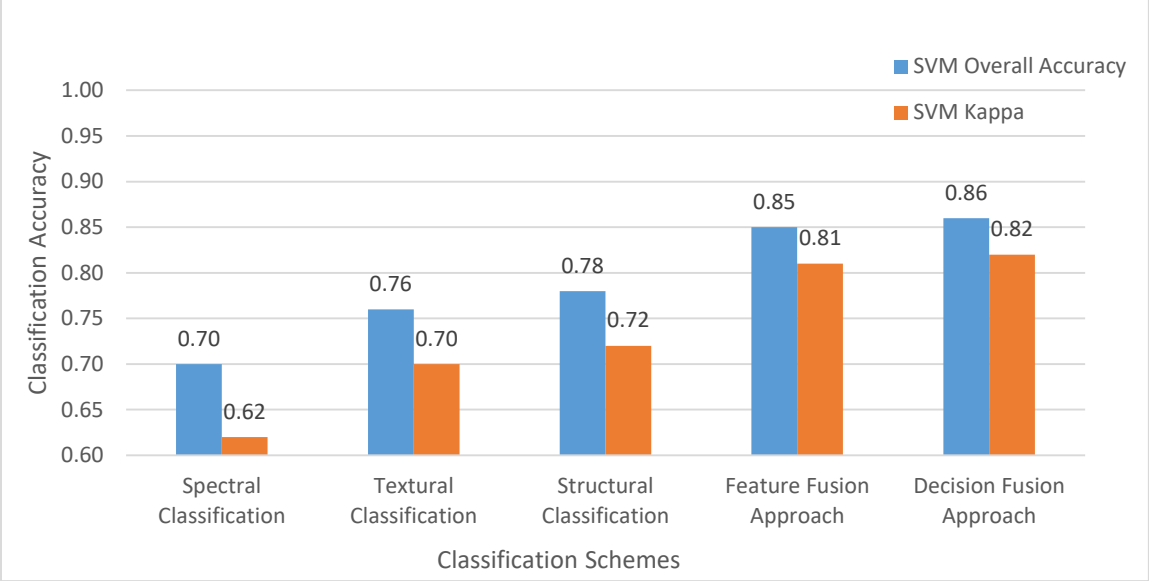

Figure 5-3 The comparison of decision fusion with other classification schemes.

Similar to feature fusion, the decision fusion approach significantly improved the classification accuracies obtained by using individual groups of features. The overall accuracies of classification schemes using spectral features, textural features, and structural features respectively were increased by 8% to 15% using the decision fusion method. Although the highest overall accuracy and kappa coefficient were achieved by the decision fusion approach, feature fusion produced comparable results with a narrow margin. This result is in accordance with recent studies on the decision fusion approach to tree species classification conducted by Aval et al. (2019) and Stavrakoudis et al. (2014). On the other hand, Hu et al. (2021) provided a mechanism to consider the uncertainties of multi-source data in decision-level fusion and obtained better classification accuracies than feature-level fusion using SVM. It is worth mentioning that the feature-level fusion decreased the performance of Hyperspectral Visible Near-Infrared (VNIR) image-based classification

(Aval et al., 2019), which might enhance the importance of the feature selection implemented before feature-level fusion in the current thesis study.

Even though comparable classification accuracies were obtained by feature-level and decision-level fusion, decision-level fusion showed advantages, as further discussed in the following by analyzing the nature of the misclassifications observed in the current study. Forty tree samples were misclassified in total, considering the classification results from both the feature-level and decision-level fusion. Among them, 25 trees were misclassified by both methods, eight by the feature fusion only and seven by the decision fusion only. The misclassification mainly occurred among honey locust, white spruce, and blue spruce, especially between blue and white spruce, as shown in the confusion matrices (Table 5-4 and Table 5-6).

Table 5-7 Classification analysis of a tree sample (white spruce) (entries highlighted in bold are predicted tree species based on the maximum probabilities for different classification schemes).

Tree ID: 705	SVM Based Posterior Probabilities				
Classification	Norway maple	honey locust	Austrian pine	blue spruce	white spruce
Spectral Feature	0.14	**0.73**	0.01	0.07	0.05
Textural Feature	0.00	0.01	0.00	**0.64**	0.35
Structural Feature	0.00	0.00	0.00	0.47	**0.53**
Feature-level fusion	0.00	0.00	0.00	0.47	**0.52**
Decision-level Fusion	0.00	0.00	0.00	**0.68**	0.32

Table 5-8 Classification analysis of a tree sample (white spruce) (entries highlighted in bold are predicted tree species based on the maximum probabilities for different classification schemes).

Tree ID: 739	SVM Based Posterior Probabilities				
Classification	Norway maple	honey locust	Austrian pine	blue spruce	white spruce
Spectral Feature	0.00	0.04	0.15	**0.72**	0.10
Textural Feature	0.00	0.01	0.04	**0.85**	0.10
Structural Feature	0.00	0.02	0.03	0.12	**0.83**
Feature-level fusion	0.00	0.00	0.11	0.41	**0.47**
Decision-level Fusion	0.00	0.00	0.00	**0.89**	0.11

The margin of a tree sample is the probability of the actual class minus the maximum value of the other classes, and the size of the margin is a measure of the degree of confidence in classification results. Among 40 misclassified samples, many misclassification results were caused by the narrow margins, indicating the uncertainties and conflicts in the classification results. Here, two misclassified examples with tree IDs of 705 and 739 were presented in Table 5-7 and Table 5-8. As shown in Table 5-7, a white spruce tree with the ID of 705 was correctly classified as white spruce with a marginal difference between the voting probabilities of only 0.05, compared with the probability of the blue spruce. On the contrary, decision-level fusion gave rise to the evidence of misclassification as blue spruce with a larger margin of 0.36, 0.68 vs. 0.32 for the probabilities. Similarly, Table 5-8 presents the misclassification analysis of another tree sample with the tree ID of 739, which was misclassified by the decision fusion but correctly

classified using feature fusion with a small margin of 0.06. On the other hand, Table 5-9 shows a positive example of the decision fusion approach. The honey locust tree with the ID of 311 was correctly classified using feature fusion and decision fusion. It is worth noting that the feature-level fusion approach successfully classified it with an even negligible margin of 0.01 between the voting probabilities of 0.49 vs. 0.48 (Austrian pine). Decision fusion enhanced the evidence of the correct classification with a slightly large margin of 0.04, 0.52 vs. 0.48 for the probabilities.

Table 5-9 Classification analysis of a tree sample (honey locust) (entries highlighted in bold are predicted tree species based on the maximum probabilities for different classification schemes).

Tree ID: 311	SVM based Posterior Probabilities				
Classification	Norway maple	honey locust	Austrian pine	blue spruce	white spruce
Spectral Feature	0.06	**0.51**	0.08	0.27	0.08
Textural Feature	0.00	0.14	**0.85**	0.00	0.00
Structural Feature	0.06	**0.47**	0.46	0.00	0.00
Feature-level fusion	0.03	**0.49**	0.48	0.00	0.00
Decision-level Fusion	0.00	**0.52**	0.48	0.00	0.00

Even though feature fusion delivered successful classifications for these tree samples, the confidence in classification accuracy is fairly weak, and the classification might be unreliable. Predicted tree species was ultimately assigned to a given tree sample based on the maximum probability for voting, even though the value might not be significantly different between two different species, which made the classification method

not robust, especially in the presence of noise added inherently by the sensors and image processing techniques. As shown in Tables 5-7, 5-8, and 5-9, the information provided by individual feature groups is often imprecise and uncertain due to the inherent conflicts among remote sensing data sources. For example, the white spruce tree was misclassified as honey locust with the probability of 0.73 and blue spruce with 0.64 using spectral features and textural features, respectively. It was indisputable that multi-source features are complementary as discussed in previous sections because sensors measure different physical properties of individual tree canopies. DST-based decision fusion approach in this study provided an effective method to combine the evidence measures from the complementary multi-source data and produced satisfactory results. However, the current method did not weigh the importance of different evidence pieces for identifying specific tree species. Hence, advanced decision rules for the decision fusion approach should be investigated in depth to adequately represent tree crowns while reducing imprecision and uncertainty.

Chapter 6 Conclusions and Future Work

In this thesis research, a DST based decision fusion approach was developed to classify five tree species at the tree crown level, specifically Norway maple, honey locust, Austrian pine, blue spruce, and white spruce, using spectral, textural, and structural features derived from MSI, high-resolution PAN, and LiDAR data, respectively. Mass functions corresponding to each feature group were determined based on the posterior probability calculated using SVM and RF algorithms, and they were combined using the Dempster Rule of combination in the decision fusion approach. When tested on the independent testing dataset, the overall classification accuracy was 86% and a kappa coefficient of 0.82 using SVM, which significantly improved the classification schemes using individual feature groups by 8% to 16% (spectral features for 70% and 0.62, textural features for 76% and 0.7, and structural features for 78% and 0.72), and slightly outperformed the commonly used feature fusion approach. In-depth analyses were also carried out to systematically explore various classification schemes combining multi-source features to identify tree species.

Advanced textural and structural features were extracted from respective PAN and LiDAR data, in addition to spectral features derived from MSI. The contribution of spectral, textural, and structural features to individual tree species classification was comprehensively analyzed based on the feature selection results and SVM and RF classification accuracies. The components of top features selected by the RFE algorithm demonstrated the complementarity of structural, textural, and spectral features in tree species classification. Nevertheless, a higher percentage of spectral and structural features

were at the top of the feature importance ranking than textural features. It is worth noting that GLCM-based features such as cluster shade and inverse difference moment exhibited significant importance in tree species classification even though they had been rarely employed in the literature. The classification results from SVM and RF showed that structural features were beneficial to the identification of tree species with widespread and dense tree crowns, such as Norway maple and honey locust, while textural features improved the classification of coniferous tree species with sparse needle leaves and small crowns such as blue spruce and white spruce. Structural features as a whole showed the most significant discriminatory power in the classification of five tree species, followed by the textural feature group. Although spectral features indicated great importance in feature importance ranking, they delivered the lowest overall classification accuracy. In particular, GLCM-based textural features contributed more than Gabor filter-derived features, whereas the 3D point distribution-related structural features were more important than the CHM-derived features.

The SVM algorithm performed consistently with RF for feature-level and decision-level approaches in the current study, although SVM showed a marginal improvement. A detailed analysis of the classification results revealed the potential of decision-level fusion in comparison to the feature-level fusion in tree species classification based on multi-source remotely sensed data. The information provided by individual feature groups was often imprecise and uncertain due to the inherent conflicts among multi-source data, which caused the low confidence in the classification results using feature fusion. DST-based decision fusion approach considered the uncertainties by quantifying the class probabilities

from individual feature groups and provided an effective method to combine the measures of evidence from the complementary multi-source data. Moreover, the decision fusion strategy based on DST holds the potential to continually improve the performance of individual tree species classification, along with comprehensive decision rules and advanced features from developed remote sensing data in the future. Therefore, the decision fusion strategy is recommended for multi-source remotely sensed data-assisted tree species classification.

Although the proposed classification framework effectively improved tree species classification using MSI, PAN, and LiDAR data, they can be further developed based on the following future considerations.

(1) The number of species types investigated was limited to five in the current study. In Toronto or other neighboring cities, there are numerous other tree species, such as bur oak (*Quercus macrocarpa*), sugar maple (*Acer saccharum*), white cedar (*Thuja occidentalis*), and sand basswood (*Tilia americana*), which dominate or co-dominate urban forests. It would be of interest to include a wide range of tree species over larger areas in future research. Caution should be made that the developed method was data-driven, and even though the framework/workflow established in this study can be used to other areas, the selected features might not be directly applied. Moreover, the classification results of a few trees are with high uncertainties reflected from the posterior probabilities generated by feature and decision fusion approaches. Trees near roads and paths are usually subject to salt, landscaping, and human interference more than those that are distant, which also increases the uncertainty for tree species classification. Tree species classes including a

two-species or a three-species compound class, and even an "unknown" class may reduce the confusion errors in other species classes, which contributes to the improvement of classifications.

(2) Additionally, the complementary features from multi-source remote sensing data have been proved to be beneficial for distinguishing tree species. However, the severe misclassification among specific tree species such as blue spruce and white spruce in this study also indicated that additional robust information is needed. Very high spatial resolution imagery acquired by Unmanned Aerial Vehicles (UAVs) and very high-density LiDAR data are capable of deriving detailed spatial and structural features to improve the classification accuracy of confusing tree species under the same genus, such as the spruce. Moreover, it is worth noting that the mismatch of the acquisition of multi-source remotely sensed data is an important factor to take into consideration when extracting multi-source features. LiDAR data used in the current study was under leaf-off condition, it would benefit the classification performance if both leaf-off and leaf-on LiDAR data were available.

(3) The DST-based decision fusion approach effectively combined the measures of evidence (probability masses in this study) from multi-source remote sensing data. Nevertheless, when significant conflicts and incompatibilities exist among the evidence, the Dempster rule combining the available evidence may result in counter-intuition decisions (Hu et al., 2021). The current method examined the uncertainties in classification results caused by conflicts among feature groups through the misclassification analysis; however, the contribution of different pieces of evidence from

multi-source to specific tree species was not weighed. Based on the current study, the decision fusion approach employing alternative combination rules or comprehensive solutions can be further explored for future considerations to deal with classification uncertainties due to the conflict information from multi-source remotely sensed data.

(4) In the current study, tree samples were manually delineated to avoid the impacts of the segmentation results on the feature extraction and thus classification performance. In future study, automatic individual tree crown (ITC) delineation will be added to the proposed workflow to make the tree species classification fully automatic.

Bibliography

Aguilar, M. A., Bianconi, F., Aguilar, F. J., & Fernández, I. (2014). Object-based greenhouse classification from GeoEye-1 and WorldView-2 stereo imagery. *Remote Sensing*, *6*(5), 3554–3582. https://doi.org/10.3390/rs6053554

Alonzo, M., Bookhagen, B., & Roberts, D. A. (2014). Urban tree species mapping using hyperspectral and lidar data fusion. *Remote Sensing of Environment*, *148*, 70–83. https://doi.org/10.1016/j.rse.2014.03.018

Asner, G. P. (1998). Biophysical and Biochemical Sources of Variability in Canopy Reflectance. *Remote Sensing of Environment*, *64*(3), 234–253. https://doi.org/https://doi.org/10.1016/S0034-4257(98)00014-5

Aval, J., Fabre, S., Zenou, E., Sheeren, D., Fauvel, M., & Briottet, X. (2019). Object-based fusion for urban tree species classification from hyperspectral, panchromatic and nDSM data. *International Journal of Remote Sensing*, *40*(14), 5339–5365. https://doi.org/10.1080/01431161.2019.1579937

Bharati, M. H., Liu, J. J., & MacGregor, J. F. (2004). Image texture analysis: Methods and comparisons. *Chemometrics and Intelligent Laboratory Systems*, *72*(1), 57–71. https://doi.org/10.1016/j.chemolab.2004.02.005

Breiman, L. (2001). Random forests. *Machine Learning*, *45*(1), 5–32. https://doi.org/10.1023/A:1010933404324

Chang, N.-B., & Bai, K. (2018). Multisensor Data Fusion and Machine Learning for Environmental Remote Sensing. In *Multisensor Data Fusion and Machine Learning for Environmental Remote Sensing*. https://doi.org/10.1201/9781315154602

Clark, M. L., & Roberts, D. A. (2012). Species-Level Differences in Hyperspectral Metrics among Tropical Rainforest Trees as Determined by a Tree-Based Classifier. *Remote Sensing*, *4*(6), 1820–1855. https://doi.org/10.3390/rs4061820

Clark, M. L., Roberts, D. A., & Clark, D. B. (2005). Hyperspectral discrimination of tropical rain forest tree species at leaf to crown scales. *Remote Sensing of Environment*, *96*(3), 375–398. https://doi.org/https://doi.org/10.1016/j.rse.2005.03.009

Clausi, D. A. (2002). An analysis of co-occurrence texture statistics as a function of grey level quantization. *Canadian Journal of Remote Sensing*, *28*(1), 45–62. https://doi.org/10.5589/m02-004

Dalponte, M., Bruzzone, L., & Gianelle, D. (2012). Tree species classification in the Southern Alps based on the fusion of very high geometrical resolution multispectral/hyperspectral images and LiDAR data. *Remote Sensing of Environment*, *123*, 258–270. https://doi.org/10.1016/j.rse.2012.03.013

Dalponte, M., Frizzera, L., & Gianelle, D. (2019). Individual tree crown delineation and tree species classification with hyperspectral and LiDAR data. *PeerJ*, *2019*(1). https://doi.org/10.7717/peerj.6227

Daugman, J. G. (1985). Uncertainty relation for resolution in space, spatial frequency, and orientation optimized by two-dimensional visual cortical filters. *Journal of the Optical Society of America. A, Optics and Image Science*, *2*(7), 1160–1169. https://doi.org/10.1364/josaa.2.001160

Demarchi, L., Kania, A., Ciezkowski, W., Piórkowski, H., Oświecimska-Piasko, Z., & Chormański, J. (2020). Recursive feature elimination and random forest classification of natura 2000 grasslands in lowland river valleys of poland based on airborne hyperspectral and LiDAR data fusion. *Remote Sensing*, *12*(11). https://doi.org/10.3390/rs12111842

Dempster, A. P. (1967). Upper and lower probabilities generated by a random closed interval. *The Annals of Mathematical Statistics*, *38*(2), 325–339. http://www.jstor.org/stable/2239772

Denisova, A. Y., Kavelenova, L. M., Korchikov, E. S., Prokhorova, N. V, Terentyeva, D. A., & Fedoseev, V. A. (2019). Tree species classification for clarification of forest inventory data using Sentinel-2 images. *Seventh International Conference on Remote Sensing and Geoinformation of the Environment (RSCy2019)*, *11174*, 1117408.

Fang, F., McNeil, B. E., Warner, T. A., & Maxwell, A. E. (2018). Combining high spatial resolution multi-temporal satellite data with leaf-on LiDAR to enhance tree species discrimination at the crown level. *International Journal of Remote Sensing*, *00*(00), 1–19. https://doi.org/10.1080/01431161.2018.1504343

Fassnacht, F. E., Latifi, H., Stereńczak, K., Modzelewska, A., Lefsky, M., Waser, L. T., Straub, C., & Ghosh, A. (2016). Review of studies on tree species classification from remotely sensed data. In *Remote Sensing of Environment* (Vol. 186, pp. 64–87). Elsevier. https://doi.org/10.1016/j.rse.2016.08.013

Felton, A., Löfroth, T., Angelstam, P., Gustafsson, L., Hjältén, J., Felton, A. M., Simonsson, P., Dahlberg, A., Lindbladh, M., & Svensson, J. (2020). Keeping pace with forestry: Multi-scale conservation in a changing production forest matrix. *Ambio*, *49*(5), 1050–1064.

Ferreira, M. P., Wagner, F. H., Aragão, L. E. O. C., Shimabukuro, Y. E., & de Souza Filho, C. R. (2019). Tree species classification in tropical forests using visible to shortwave infrared WorldView-3 images and texture analysis. *ISPRS Journal of Photogrammetry and Remote Sensing*, *149*(August 2018), 119–131. https://doi.org/10.1016/j.isprsjprs.2019.01.019

Fitzky, A. C., Sandén, H., Karl, T., Fares, S., Calfapietra, C., Grote, R., ... & Rewald, B. (2019). The interplay between ozone and urban vegetation—BVOC emissions, ozone deposition, and tree ecophysiology. *Frontiers in Forests and Global Change*, 2, 50. https://doi.org/10.3389/ffgc.2019.00050

Franklin, S. E., Maudie, A. J., Lavigne, M. B., & others. (2001). Using spatial co-occurrence texture to increase forest structure and species composition classification accuracy. *Photogrammetric Engineering and Remote Sensing*, *67*(7), 849–856.

Georganos, S., Grippa, T., Vanhuysse, S., Lennert, M., Shimoni, M., Kalogirou, S., & Wolff, E. (2018). Less is more: optimizing classification performance through feature selection in a very-high-resolution remote sensing object-based urban application. *GIScience and Remote Sensing*, *55*(2), 221–242. https://doi.org/10.1080/15481603.2017.1408892

Ghassemian, H. (2016). A review of remote sensing image fusion methods. *Information Fusion*, *32*, 75–89. https://doi.org/10.1016/j.inffus.2016.03.003

Gillespie, T. W., de Goede, J., Aguilar, L., Jenerette, G. D., Fricker, G. A., Avolio, M. L., Pincetl, S., Johnston, T., Clarke, L. W., & Pataki, D. E. (2017). Predicting tree species richness in urban forests. *Urban Ecosystems*, *20*(4), 839–849.

Gitelson, A., & Merzlyak, M. N. (1994). Quantitative estimation of chlorophyll-a using reflectance spectra: Experiments with autumn chestnut and maple leaves. *Journal of Photochemistry and Photobiology B: Biology*, *22*(3), 247–252. https://doi.org/https://doi.org/10.1016/1011-1344(93)06963-4

Gregorutti, B., Michel, B., & Saint-Pierre, P. (2017). Correlation and variable importance in random forests. *Statistics and Computing*, *27*(3), 659–678. https://doi.org/10.1007/s11222-016-9646-1

Guyon, I., & Elisseeff, A. (2003). An introduction to variable and feature selection. *Journal of Machine Learning Research*, *3*(Mar), 1157–1182.

Haghighat, M., Zonouz, S., & Abdel-Mottaleb, M. (2013). Identification using encrypted biometrics. *International Conference on Computer Analysis of Images and Patterns*, 440–448.

Han, H., Guo, X., & Yu, H. (2016). Variable selection using Mean Decrease Accuracy and Mean Decrease Gini based on Random Forest. *Proceedings of the IEEE International Conference on Software Engineering and Service Sciences, ICSESS*, 219–224. https://doi.org/10.1109/ICSESS.2016.7883053

Hansch, R., & Hellwich, O. (2020). Fusion of Multispectral LiDAR, Hyperspectral, and RGB Data for Urban Land Cover Classification. *IEEE Geoscience and Remote Sensing Letters*, 1–5. https://doi.org/10.1109/lgrs.2020.2972955

Haralick, R. M., Shanmugam, K., & Dinstein, I. H. (1973). Textural features for image classification. *IEEE Transactions on Systems, Man, and Cybernetics*, *6*, 610–621. https://ieeexplore.ieee.org/document/4309314

Hartling, S., Sagan, V., & Maimaitijiang, M. (2021). Urban tree species classification using UAV-based multi-sensor data fusion and machine learning. *GIScience and Remote Sensing*, *58*(8), 1250–1275. https://doi.org/10.1080/15481603.2021.1974275

Hartling, S., Sagan, V., Sidike, P., Maimaitijiang, M., & Carron, J. (2019). Urban tree species classification using a worldview-2/3 and liDAR data fusion approach and deep learning. *Sensors (Switzerland)*, *19*(6), 1–23. https://doi.org/10.3390/s19061284

Heiskanen, J., Korhonen, L., Hietanen, J., & Pellikka, P. K. E. (2015). Use of airborne lidar for estimating canopy gap fraction and leaf area index of tropical montane forests. *International Journal of Remote Sensing*, *36*(10), 2569–2583. https://doi.org/10.1080/01431161.2015.1041177

Hu, B., Li, Q., & Hall G., B. (2021). A decision-level fusion approach to tree species classification from multi-source remotely sensed data. *ISPRS Open Journal of Photogrammetry and Remote Sensing*, *1*(July), 100002. https://doi.org/10.1016/j.ophoto.2021.100002

Huang, X. (2019). *Single tree urban inventory updates* [Master's thesis, University of Toronto]. University of Toronto Digital Assets. https://hdl.handle.net/1807/93303

Huete, A., Didan, K., Miura, T., Rodriguez, E. ., Gao, X., & Ferreira, L. . (2002). Overview of the radiometric and biophysical performance of the MODIS vegetation indices. *Remote Sensing of Environment*, *83*(1–2), 195–213. https://doi.org/10.1016/S0034-4257(02)00096-2

Joshi, N., Baumann, M., Ehammer, A., Fensholt, R., Grogan, K., Hostert, P., Jepsen, M. R., Kuemmerle, T., Meyfroidt, P., Mitchard, E. T. A., Reiche, J., Ryan, C. M., & Waske, B. (2016). A review of the application of optical and radar remote sensing data fusion to land use mapping and monitoring. *Remote Sensing*, *8*(1), 1–23. https://doi.org/10.3390/rs8010070

Karatzoglou, A., Meyer, D., & Hornik, K. (2006). Support Vector Algorithm in R. *Journal of Statistical Software*, *15*(9), 1–28.

Kashani, A. G., Olsen, M. J., Parrish, C. E., & Wilson, N. (2015). A review of LiDAR radiometric processing: From ad hoc intensity correction to rigorous radiometric calibration. *Sensors*, *15*(11), 28099–28128. https://doi.org/10.3390/s151128099

Korpela, I., Ørka, H. O., Maltamo, M., Tokola, T., Hyyppä, J., & others. (2010). Tree species classification using airborne LiDAR--effects of stand and tree parameters, downsizing of training set, intensity normalization, and sensor type. *Silva Fennica*, *44*(2), 319–339. https://doi.org/10.14214/sf.156

Kuhn, M. (2008). Building Predictive Models in R Using the caret Package. *Journal of Statistical Software*, *28*(5), 1–26. https://doi.org/10.18637/JSS.V028.I05

Kukunda, C. B., Duque-Lazo, J., González-Ferreiro, E., Thaden, H., & Kleinn, C. (2018). Ensemble classification of individual Pinus crowns from multispectral satellite imagery and airborne LiDAR. *International Journal of Applied Earth Observation and Geoinformation*, *65*(July 2017), 12–23. https://doi.org/10.1016/j.jag.2017.09.016

Landis, J. R., & Koch, G. G. (1977). The Measurement of Observer Agreement for Categorical Data. *Biometrics*, *33*(1), 159. https://doi.org/10.2307/2529310

Larrubia, C. J., Kane, K. R., Wolfslehner, B., Guldin, R., & Rametsteiner, E. (2017). Using criteria and indicators for sustainable forest management: a way to strengthen results-based management of national forest programmes. *Forestry Policy and Institutions Working Paper-Food and Agriculture Organization*, *37*. http://www.fao.org/3/a-i6883e.pdf

Li, D., Ke, Y., Gong, H., & Li, X. (2015). Object-based urban tree species classification using bi-temporal worldview-2 and worldview-3 images. *Remote Sensing*, *7*(12), 16917–16937. https://doi.org/10.3390/rs71215861

Li, H., Hu, B., Li, Q., & Jing, L. (2020). CNN-Based Tree Species Classification Using Airborne Lidar Data and High-Resolution Satellite Image. *International Geoscience and Remote Sensing Symposium (IGARSS)*, 2679–2682. https://doi.org/10.1109/IGARSS39084.2020.9324011

Li, J., & Hu, B. (2012). Exploring high-density airborne light detection and ranging data for classification of mature coniferous and deciduous trees in complex Canadian forests. *Journal of Applied Remote Sensing*, *6*(1), 63536. https://doi.org/10.1117/1.JRS.6.063536

Li, J., Hu, B., & Noland, T. L. (2013). Classification of tree species based on structural features derived from high density LiDAR data. *Agricultural and Forest Meteorology*, *171–172*, 104–114. https://doi.org/10.1016/j.agrformet.2012.11.012

Li, J., Hu, B., & Woods, M. (2015). A Two-Level Approach for Species Identification of Coniferous Trees in Central Ontario Forests Based on Multispectral Images. *IEEE Journal of Selected Topics in Applied Earth Observations and Remote Sensing*, *8*(4), 1487–1497. https://doi.org/10.1109/JSTARS.2015.2423272

Liaw, A., & Wiener, M. (2002). Classification and regression by randomForest. R news, 2(3), 18-22.

Lin, H., Lin, C., & Weng, R. (2007). A note on Platt's probabilistic outputs for support vector machines. *Machine Learning*, *68*(3), 267–276. https://doi.org/10.1007/s10994-007-5018-6

Lin, Y., & Hyyppä, J. (2016). A comprehensive but efficient framework of proposing and validating feature parameters from airborne LiDAR data for tree species classification. *International Journal of Applied Earth Observation and Geoinformation*, *46*, 45–55. https://doi.org/10.1016/j.jag.2015.11.010

Lin, Y., & Martin, H. (2016). Tree species classification based on stem-related feature parameters derived from static terrestrial laser scanning data. *Agricultural and Forest Meteorology*, *37*(18), 105–114. https://doi.org/10.1080/01431161.2016.1213920

Liu, L., Coops, N. C., Aven, N. W., & Pang, Y. (2017). Mapping urban tree species using integrated airborne hyperspectral and LiDAR remote sensing data. *Remote Sensing of Environment*, *200*(July), 170–182. https://doi.org/10.1016/j.rse.2017.08.010

Madonsela, S., Cho, M. A., Ramoelo, A., & Mutanga, O. (2017). Remote sensing of species diversity using Landsat 8 spectral variables. *ISPRS Journal of Photogrammetry and Remote Sensing*, *133*, 116–127. https://doi.org/10.1016/j.isprsjprs.2017.10.008

Marrs, J., & Ni-Meister, W. (2019). Machine learning techniques for tree species classification using co-registered LiDAR and hyperspectral data. *Remote Sensing*, *11*(7), 1–18. https://doi.org/10.3390/rs11070819

Maxwell, A. E., Warner, T. A., & Fang, F. (2018). Implementation of machine-learning classification in remote sensing: An applied review. *International Journal of Remote Sensing*, *39*(9), 2784–2817. https://doi.org/10.1080/01431161.2018.1433343

Meyer, D. and Wien, F.T. (2021) Support Vector Machines. The Interface to Libsvm in Package, e1071. https://cran.r-project.org/web/packages/e1071/vignettes/svmdoc.pdf

Meyer, D., Dimitriadou, E., Hornik, K., Weingessel, A., & Leisch, F. (2021). *e1071: Misc Functions of the Department of Statistics, Probability Theory Group (Formerly: E1071)*, TU Wien, 2018, R package version 1.7-0.

Mojaddadi Rizeei, H., Pradhan, B., & Saharkhiz, M. A. (2019). Urban object extraction using Dempster Shafer feature-based image analysis from worldview-3 satellite imagery. *International Journal of Remote Sensing*, *40*(3), 1092–1119. https://doi.org/10.1080/01431161.2018.1524173

Morgenroth, J., Östberg, J., Konijnendijk van den Bosch, C., Nielsen, A. B., Hauer, R., Sjöman, H., Chen, W., & Jansson, M. (2016). Urban tree diversity—Taking stock and looking ahead. *Urban Forestry & Urban Greening*, *15*, 1–5. https://doi.org/https://doi.org/10.1016/j.ufug.2015.11.003

Mountrakis, G., Im, J., & Ogole, C. (2011). Support vector machines in remote sensing: A review. *ISPRS Journal of Photogrammetry and Remote Sensing*, *66*(3), 247–259. https://doi.org/10.1016/j.isprsjprs.2010.11.001

Paap, T., Burgess, T. I., & Wingfield, M. J. (2017). Urban trees: bridge-heads for forest pest invasions and sentinels for early detection. *Biological Invasions*, *19*(12), 3515–3526. https://doi.org/10.1007/s10530-017-1595-x

Piiroinen, R., Fassnacht, F. E., Heiskanen, J., Maeda, E., Mack, B., & Pellikka, P. (2018). Invasive tree species detection in the Eastern Arc Mountains biodiversity hotspot using one class classification. *Remote Sensing of Environment*, *218*, 119–131. https://doi.org/10.1016/j.rse.2018.09.018

Platt, J. (1999). Probabilistic outputs for support vector machines and comparisons to regularized likelihood methods. *Advances in Large Margin Classifiers*, *10*(3), 61–74.

Pohl, C., & Van Genderen, J. L. (1998). Review article multisensor image fusion in remote sensing: concepts, methods and applications. *International Journal of Remote Sensing*, *19*(5), 823–854. https://doi.org/10.1080/014311698215748

Pu, R., & Landry, S. (2012). A comparative analysis of high spatial resolution IKONOS and WorldView-2 imagery for mapping urban tree species. *Remote Sensing of Environment*, *124*, 516–533. https://doi.org/10.1016/j.rse.2012.06.011

Puttonen, E., Suomalainen, J., Hakala, T., Räikkönen, E., Kaartinen, H., Kaasalainen, S., & Litkey, P. (2010). Tree species classification from fused active hyperspectral reflectance and LIDAR measurements. *Forest Ecology and Management*, *260*(10), 1843–1852. https://doi.org/https://doi.org/10.1016/j.foreco.2010.08.031

Raczko, E., & Zagajewski, B. (2017). Comparison of support vector machine, random forest and neural network classifiers for tree species classification on airborne hyperspectral APEX images. *European Journal of Remote Sensing*, *50*(1), 144–154. https://doi.org/10.1080/22797254.2017.1299557

Ramakrishnan, A. G., Raja, S., & Ram, H. V. R. (2002). Neural network-based segmentation of textures using Gabor features. *Proceedings of the 12th IEEE Workshop on Neural Networks for Signal Processing*, 365–374.

Reitberger, J., Krzystek, P., & Stilla, U. (2008). Analysis of full waveform LIDAR data for the classification of deciduous and coniferous trees. *International Journal of Remote Sensing*, *29*(5), 1407–1431. https://doi.org/10.1080/01431160701736448

Rondeaux, G., Steven, M., & Baret, F. (1996). Optimization of soil-adjusted vegetation indices. *Remote Sensing of Environment*, *55*(2), 95–107. https://doi.org/https://doi.org/10.1016/0034-4257(95)00186-7

Rouse, J. W., Haas, R. H., Schell, J. A., & Deering, D. W. (1974). Monitoring vegetation systems in the Great Plains with ERTS: Proceedings of the Third Earth Resources Technology Satellite-1 Symposium. *NASA SP-351*, 301–317.

Saeidi, V., Pradhan, B., Idrees, M. O., & Latif, Z. A. (2014). Fusion of airborne LiDAR with multispectral SPOT 5 image for enhancement of feature extraction using dempster-shafer theory. *IEEE Transactions on Geoscience and Remote Sensing*, *52*(10), 6017–6025. https://doi.org/10.1109/TGRS.2013.2294398

Schmitt, M., & Zhu, X. X. (2016). Data Fusion and Remote Sensing: An ever-growing relationship. *IEEE Geoscience and Remote Sensing Magazine*, *4*(4), 6–23. https://doi.org/10.1109/MGRS.2016.2561021

Shafer, G. (1976). *A mathematical theory of evidence* (Vol. 42). *Princeton University Press*. https://doi.org/10.1515/9780691214696

Shi, Y., Skidmore, A. K., Wang, T., Holzwarth, S., Heiden, U., Pinnel, N., Zhu, X., & Heurich, M. (2018). Tree species classification using plant functional traits from LiDAR and hyperspectral data. *International Journal of Applied Earth Observation and Geoinformation*, *73*(May), 207–219. https://doi.org/10.1016/j.jag.2018.06.018

Shi, Y., Wang, T., Skidmore, A. K., & Heurich, M. (2018). Important LiDAR metrics for discriminating forest tree species in Central Europe. *ISPRS Journal of Photogrammetry and Remote Sensing*, *137*, 163–174. https://doi.org/10.1016/j.isprsjprs.2018.02.002

Shojanoori, R., & Shafri, H. Z. M. (2016). Review on the use of remote sensing for urban forest monitoring. *Arboriculture and Urban Forestry*, *42*(6), 400–417. https://doi.org/10.48044/jauf.2016.034

Spanner, M. A., Pierce, L. L., Peterson, D. L., & Running, S. W. (1990). Remote sensing of temperate coniferous forest leaf area index The influence of canopy closure, understory vegetation and background reflectance. *International Journal of Remote Sensing*, *11*(1), 95–111. https://doi.org/10.1080/01431169008955002

Stavrakoudis, D. G., Dragozi, E., Gitas, I. Z., & Karydas, C. G. (2014). Decision fusion based on hyperspectral and multispectral satellite imagery for accurate forest species mapping. *Remote Sensing*, *6*(8), 6897–6928. https://doi.org/10.3390/rs6086897

Stehman, S. V. (1997). Selecting and interpreting measures of thematic classification accuracy. *Remote Sensing of Environment*, *62*(1), 77–89. https://doi.org/https://doi.org/10.1016/S0034-4257(97)00083-7

Tigges, J., Lakes, T., & Hostert, P. (2013). Urban vegetation classification: Benefits of multitemporal RapidEye satellite data. *Remote Sensing of Environment*, *136*, 66–75. https://doi.org/10.1016/j.rse.2013.05.001

Wang, K., Wang, T., & Liu, X. (2018). A Review: Individual Tree Species Classification Using Integrated Airborne LiDAR and Optical Imagery with a Focus on the Urban Environment. *Forests*, *10*(1), 1. https://doi.org/10.3390/f10010001

Waser, L. T., Küchler, M., Jütte, K., & Stampfer, T. (2014). Evaluating the potential of worldview-2 data to classify tree species and different levels of ash mortality. *Remote Sensing*, *6*(5), 4515–4545. https://doi.org/10.3390/rs6054515

Wu, C., Gonsamo, A., Gough, C. M., Chen, J. M., & Xu, S. (2014). Modeling growing season phenology in North American forests using seasonal mean vegetation indices from MODIS. *Remote Sensing of Environment*, *147*, 79–88. https://doi.org/10.1016/j.rse.2014.03.001

Wu, T.-F., Lin, C.-J., & Weng, R. (2003). Probability estimates for multi-class classification by pairwise coupling. *Advances in Neural Information Processing Systems*, *16*.

Wu, Y., & Zhang, X. (2020). Object-Based tree species classification using airborne hyperspectral images and LiDAR data. *Forests*, *11*(1). https://doi.org/10.3390/f11010032

Yang, G., Zhao, Y., Li, B., Ma, Y., Li, R., Jing, J., & Dian, Y. (2019). Tree species classification by employing multiple features acquired from integrated sensors. *Journal of Sensors*, *2019*. https://doi.org/10.1155/2019/3247946

Yao, W., Krzystek, P., & Heurich, M. (2012). Tree species classification and estimation of stem volume and DBH based on single tree extraction by exploiting airborne full-waveform LiDAR data. *Remote Sensing of Environment*, *123*, 368–380. https://doi.org/https://doi.org/10.1016/j.rse.2012.03.027

Zhang, J. (2010). Multi-source remote sensing data fusion: Status and trends. *International Journal of Image and Data Fusion*, *1*(1), 5–24. https://doi.org/10.1080/19479830903561035

Zheng, D., Zhao, Y., & Wang, J. (2004). Features extraction using a Gabor filter family. *Sixth IASTED International Conference on Signal and Image Processing*, 139–144.

Publications

Portions of the results from this thesis research have been published in the following journal papers:

Hu, B., Li, Q., & Hall, G. B. (2021). A decision-level fusion approach to tree species classification from multi-source remotely sensed data, ISPRS Open Journal of Photogrammetry and Remote Sensing, Volume 1, 2021, 100002, ISSN 2667-3932. https://doi.org/10.1016/j.ophoto.2021.100002.

Li, H., Hu, B., Li, Q., & Jing, L. (2021). CNN-Based Individual Tree Species Classification Using High-Resolution Satellite Imagery and Airborne LiDAR Data. Forests 2021, 12(12), 1697.https://doi.org/10.3390/f12121697.

Hu, B. and Q. Li (2021). Tree species classification based on neutrosophic logic and Dempster-Shafer theory. The ISPRS Annals of the Photogrammetry, Remote Sensing and Spatial Information Sciences.

For these papers, I processed the multispectral imagery, LiDAR data and the image co-registration, and established tree species sample set, and performed the multi-source feature extraction and classification models using machine learning algorithms.